Agricultural and Forest Meteorology 347 (2024) 109915

Contents lists available at ScienceDirect

Agricultural and Forest Meteorology

journal homepage: www.elsevier.com/locate/agrformet

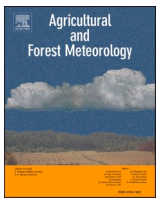

Meteorological control on snow depth evolution and snowpack energy exchanges in an agro-forested environment by a measurement-based approach: A case study in Sainte-Marthe, Eastern Canada

Vasana Dharmadasa [a,b,c,*], Christophe Kinnard [a,b,c], Michel Baraër [d]

[a] Department of Environmental Sciences, University of Québec at Trois-Rivières, QC G8Z 4M3, Canada
[b] Center for Northern Studies (CEN), Québec City, QC GV1 0A6, Canada
[c] Research Centre for Watershed-Aquatic Ecosystem Interactions (RIVE), University of Québec at Trois-Rivières, Trois-Rivières, QC G8Z 4M3, Canada
[d] Department of Construction Engineering, École de technologie supérieure, Montréal, QC H3C 1K3, Canada

ARTICLE INFO

Keywords:
Snow energy budget
Agro-forested environment
Blowing snow

ABSTRACT

A lack of field studies measuring snow mass and energy balance in open and forest patches hinders the holistic understanding of snowpack dynamics and makes it difficult to validate modeling efforts in agro-forested environments. In such context, this study explores the energy exchanges within snowpacks in an agro-forested environment in eastern Canada, with a focus on measuring energy fluxes and assessing temporal variability and meteorological controls on the snowpack. The results showed that there are considerable differences in energy fluxes between open, forest, and gap areas, with net radiation dominating the snow surface energy balance. During the accumulation period, longwave radiation had a greater influence on the variability of the energy balance, while during the ablation period, latent heat fluxes and solar radiation absorption dominated the variability of the energy balance and snowpack melting. Blowing snow also influenced the energy budget in the open area through negative feedback effects. Despite the negative feedback effects, results showed that the decreased air stability in response to the reduced temperature gradient between the atmosphere and snowpack counterbalanced the reduced vapor pressure gradient and resulted in slightly increased latent heat (sublimation) losses from the snowpack during blowing snow. Furthermore, our analysis showed reduced influxes of sensible heat and longwave radiation to the snowpack in response to the blowing snow cooling feedback on the atmosphere. These results emphasize the significant role of blowing snow for the energy exchanges in large wind-exposed open areas in humid continental agro-forested landscapes. Furthermore, the different snowpack and energy balance conditions between the open and forested patches of agro-forested landscapes highlighted in this study could have important implications for snowmelt infiltration patterns and resulting catchment-scale hydrology.

1. Introduction

Snow cover is an integral component of the climate system in cold climate regions. It represents a major part of the terrestrial water storage during the winter season and produces a significant spring runoff with the onset of snowmelt. Snow accumulation and the timing, intensity, and duration of snowmelt depend on meteorological and physiographic variables such as regional climate, elevation, vegetation presence/absence, and forest structure (Golding and Swanson, 1986; Elder et al., 1998; Pomeroy et al., 1998a; Roth and Nolin, 2017; Zheng et al., 2018). Snowpack energy budget is a key element to understand the spatial and temporal evolution of snowpack in different climatic and physiographic settings. For instance, compared to open areas, forest cover reduces the incoming shortwave radiation, increases longwave radiation, dampens wind speed, and hence reduces turbulent heat transfers within the canopy (Prévost et al., 1991; Pomeroy and Gray, 1994; Tarboton, 1994; Pomeroy and Dion, 1996; Pomeroy and Granger, 1997; Pomeroy et al., 1998a, 1998b; Helgason and Pomeroy, 2012a). In turn, the snowpack dynamics within a forest differ from that in an open area. A significant amount of literature reported reduced snow accumulation in forested areas compared to adjacent open areas due to canopy interception and sublimation losses and slower snowmelt rates in spring due to shading

* Corresponding author.
E-mail address: vasana.sandamali.dharmadasa@uqtr.ca (V. Dharmadasa).

https://doi.org/10.1016/j.agrformet.2024.109915
Received 4 April 2023; Received in revised form 21 December 2023; Accepted 29 January 2024
Available online 2 February 2024

by the canopy, or, in a humid climate, faster snowmelt due to increased longwave radiation with higher canopy density- the 'radiative paradox' (Pomeroy and Granger, 1997; Hopkinson et al., 2004; Varhola et al., 2010; Lundquist et al., 2013; Zheng et al., 2018; Hojatimalekshah et al., 2021). Snow accumulation and melt also differ significantly between different forest stands with distinct structural differences, due to the impact of forest structure on the energy balance, dominated by radiative heat fluxes (Winkler et al., 2005). Accumulation and melt rates generally decline with increasing canopy density and leaf area (Pomeroy et al., 2002). For example, larger canopy interception and losses in coniferous forests result in less snow on the ground than that in deciduous and mixed forests (Hopkinson et al., 2012; Aygün et al., 2020). Open areas on the other hand are generally characterized by large fetch distances and high wind speeds that promote erosion of the snow cover by increased blowing snow fluxes and sublimation losses (Pomeroy and Gray, 1994). High wind speeds also significantly increase turbulent energy exchanges in open areas which eventually increase snow sublimation (Roth and Nolin, 2017). The importance of blowing snow fluxes in shaping the open terrain snow cover and its ultimate influence on the magnitude and timing of snowmelt has been well documented (Pomeroy and Gray, 1994; Pomeroy et al., 1998a; Prasad et al., 2001; Essery and Pomeroy, 2004; Liston et al., 2007; Mott et al., 2018). For example, in the Canadian prairies, 8–19% of annual snowfall is removed by blowing snow fluxes (by saltation and suspension), and 15–40% or more of annual snowfall is lost through blowing snow sublimation (Pomeroy et al., 1993; Pomeroy and Gray, 1995). Several authors reported substantial differences in snow accumulation and melt in forest clearings or gaps compared to adjacent forests and open areas (e.g., Troendle and Leaf, 1980; Golding and Swanson, 1986; Swanson, 1988; Pomeroy and Gray, 1994; Pomeroy et al., 2002; Woods et al., 2006; Pomeroy et al., 2012; Broxton et al., 2015; Conway et al., 2018). Collectively, they demonstrate that small gaps (~2–5 times the tree height diameter) are often still sheltered by trees, while large gaps are exposed to wind erosion that eventually reduces the overall snow accumulation.

The knowledge on energy exchanges between the snowpack, atmosphere, and the ground is important for the prediction of snowmelt rates in hydrological applications (Mas et al., 2018), determination of land surface-atmosphere interactions for climate modeling and weather forecasting (Pomeroy et al., 1998a), and prediction of avalanche hazards (Brun et al., 1989). Indeed, many of the snow physics models developed for such applications are based on energy budget estimation. Since their early developments, these models have been greatly improved with the addition of new parameterizations for turbulent energy transfer (Andreas et al., 2010), blowing snow (Pomeroy et al., 1993; Liston et al., 2007; Pomeroy et al., 2007), and snow metamorphism (Lehning et al., 2002). However, despite these advances, in a snowmelt model intercomparison project, Rutter et al. (2009) reported that snowmelt models do not consistently produce acceptable results in all environments. This is partly due to the inability to robustly simulate the snowpack processes and snow-atmosphere-ground interactions (Rutter et al., 2009). However, the availability of calibration data could solve a major portion of this issue by reducing the parameter uncertainty and thereby offsetting model deficiencies (Essery et al., 2009). This highlights the importance of having detailed meteorological and/or energy flux measurements in different environments.

The snowpack energy exchanges in different environments are well documented in large open areas like the Canadian prairies (Pomeroy et al., 1993; Pomeroy and Gray, 1994; Pomeroy et al., 1998a; Harder et al., 2017, 2018) and Arctic (Price and Dunne, 1976; Liston and Sturm, 1998; Boike et al., 2003; Lackner et al., 2022), forested environments (Barry et al., 1990; Prévost et al., 1991; Pomeroy and Granger, 1997; Lundquist et al., 2013), and mountainous regions (Kuipers Munneke et al., 2009; Mott et al., 2011b; Helgason and Pomeroy, 2012b; Mott et al., 2017; Roth and Nolin, 2017; Bair et al., 2018; Hoelzle et al., 2022). Collectively, these studies show marked differences in snow mass and energy fluxes in different environments depending on vegetation and topographical settings, which in turn have a substantial effect on snowmelt and regional hydrology. On the other hand, agro-forested catchments, which are composed of alternate patches of open lands (mostly agricultural) and forest, have been little studied. Snow-affected agro-forested landscapes characterize much of eastern Canada (Jobin et al., 2014), but also part of the Midwest and northeastern USA (Gootman and Hubbart, 2021; Jacobs et al., 2021), and northern Europe (Luomaranta et al., 2019). Differences in snow mass and energy balance within agro-forested environments would be expected to exert a significant influence on regional hydrology (Aygün et al., 2020, 2022). However, the lack of field studies simultaneously measuring snow mass and energy balance in open and forest patches hampers the holistic understanding of snowpack dynamics and makes it difficult to validate the modeling efforts in these agro-forested landscapes (Brown, 2010; Sena et al., 2017; Aygün et al., 2020; Paquotte and Baraer, 2021). Therefore, the objective of this study is to simultaneously measure energy fluxes and assess the temporal variability and meteorological controls on snow energy transfer between open ground, forest, and forest clearing (gap) within an agro-forested environment in eastern Canada. We hypothesize that these predominant but different land cover and uses will strongly modify the radiative and turbulent heat exchanges at the snow-atmosphere interface due to canopy effects on radiation and wind speed. We also present the first measurements of blowing snow fluxes in this kind of environment and investigate weather conditions associated with blowing snow events, as well as how blowing snow fluxes impact the energy budget, which is largely understudied in agro-forested, humid continental climates. We specifically test the hypothesis that blowing snow events under snowfall-free conditions modify the latent heat and sensible heat exchanges calculated by the bulk aerodynamic method, which was shown by previous modeling studies (e.g., Déry et al., 1998; Vionnet et al., 2014; Le Toumelin et al., 2021). In view of the lack of observational studies, our study is expected to provide a baseline for energy partitioning in agro-forested landscapes using a measurement-based approach that would benefit future modeling applications.

2. Study sites and measurements

The study was conducted at three sites within the experimental watershed of Sainte-Marthe in southern Québec, eastern Canada (Fig. 1). The watershed has an extent of 9 km^2 with a mixed wood forest in the upper catchment and agricultural areas downstream. The climate of the region is characterized by a sub-humid continental climate (Paquotte and Baraer, 2021; Valence et al., 2022). Automatic weather station (AWS) measurements from three contrasted sites were used in this study: (i) an "open" site located in an open agricultural area (45.40°N, 74.31°W), (ii) a "forest" site in the mixed wood forest (mostly deciduous, 45.43°N, 74.28°W), and (iii) a "gap" site in a clearing zone of approximately 20 × 30 m in the mixed wood forest area (45.42°N, 74.28°W). Although the open station is located a little outside the watershed boundary due to logistical reasons, it shares the same climatic conditions. Also, the proximity of the sites and their similar topographic settings (flat, within an elevation range of 69–110 m asl (above sea level)), allow isolating the effect of land use on the snow energy and mass balance. The gap station has been in operation since 2016 and the open and forest stations have been operational since December 2019. Fig. 1 shows the study locations and Table 1 outlines the details of the individual measurements at each site.

All data were recorded at hourly intervals using a CR3000 data logger (Campbell Scientific) in the open, at hourly intervals using a CR1000 data logger in the forest, and at 15 min intervals using a CR1000 data logger in the gap. Temperatures within the snowpack were measured from 0 to +30 cm at a 10 cm interval. Ground temperatures were measured at depths from 0 to –60 cm at a 10 cm interval and ground volumetric water content was measured from 0 to –40 cm at the same interval. Ground temperature and soil moisture sensors in the

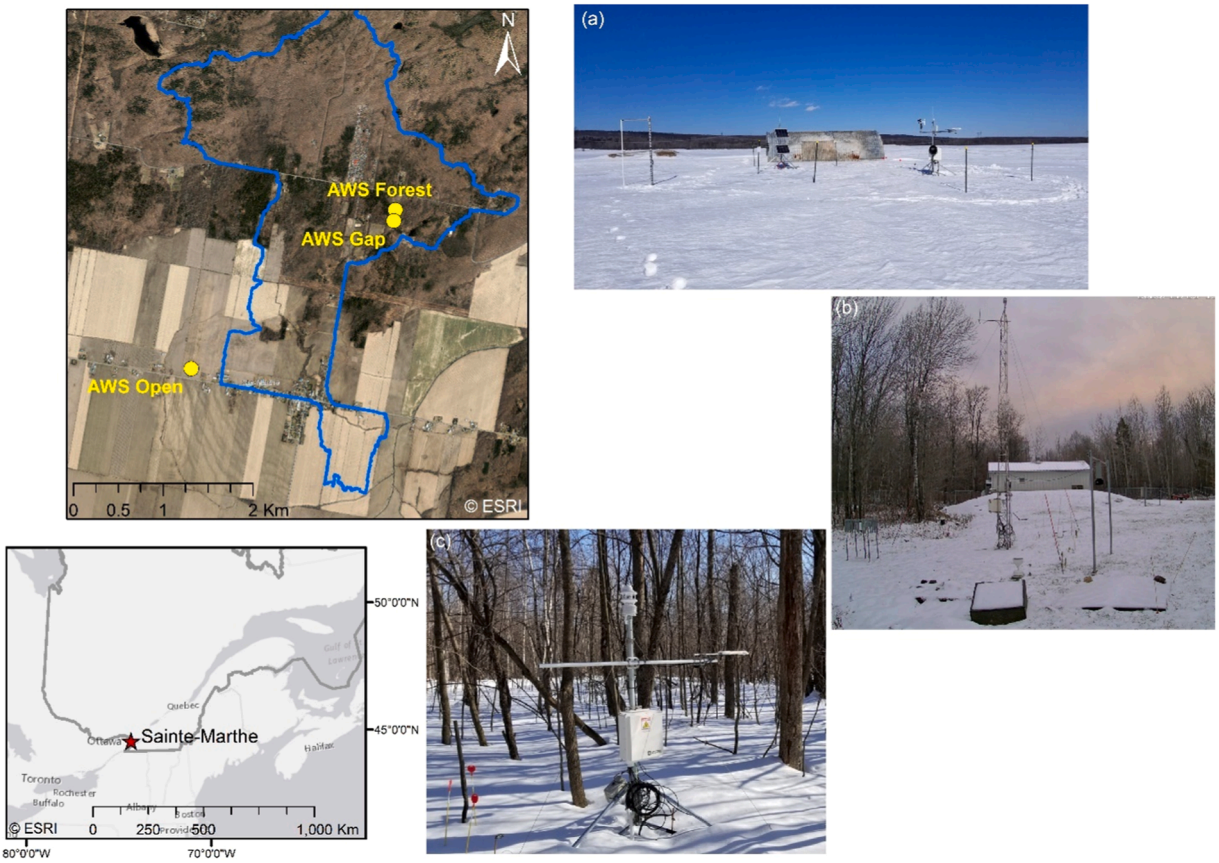

Fig. 1. Study site locations in the Sainte-Marthe watershed a) open; b) gap; and c) forest. Note that the building visible in gap site (Fig. 1b) is not likely to influence the wind measurements as it is located far enough from the sensors (~26 m) and downwind of the site.

Table 1
List of instruments used and their characteristics at the three different sites.

Parameters	Sensors	Manufacturer	Range	Accuracy	Station
Shortwave and longwave radiation	Pyranometer and pyrgeometer (CNR4)	Kipp & Zonen	0.3–2.8 μm, 4.5–42 μm	±10% [a], ±10% [a]	Open Gap Forest
Air Temperature and relative humidity	HMP155A probe	Vaisala	–80–60 °C, 0–100%	±0.5 °C, ±1.5%	Open
	Platinum thermocouple HygroClip (HC-S3L)	Rotronic Instrument Corp	–40–60 °C, 0–100%	±0.6 °C, ±1.5%	Gap
	WS700-UMB	Lufft	–50–60 °C, 0–100%	±0.2 °C, ±2%	Forest
Atmospheric pressure	Barometer (CS106)	Vaisala	500–1100 hPa	±1.5 hPa	Open
	Barometer (CS106)	Vaisala	500–1100 hPa	±1.5 hPa	Gap
	WS700-UMB	Lufft	300–1200 hPa	±0.5 hPa	Forest
Wind speed and wind direction	Anemometer (5103-L)	R. M. Young	0–100 m s^{-1}, 0–360 °	±0.3 m s^{-1}, ±3 °	Open
	Anemometer (5103-L)	R. M. Young	0–100 m s^{-1}, 0–360 °	±0.3 m s^{-1}, ±3 °	Gap
	WS700-UMB	Lufft	0–100 m s^{-1}, 0–360 °	±0.3 m s^{-1}, < 3 °	Forest
Precipitation	WS700-UMB	Lufft	0.3–5 mm drop size 0–200 mm h^{-1} intensity	±2%	Gap
Snow depth	Sonic telemetry sensor (SR50A)	Campbell Scientific	0.5–10 m	±1 cm	Open Gap Forest
Snow and ground temperatures	Temperature probes (107)	Campbell Scientific	–35–50 °C	±0.2 °C	Open Gap Forest
Soil moisture (volumetric water content)	Reflectometer (CS-655)	Campbell Scientific	0–100%	±1 or ± 3%	Open Gap
Blowing snow	FlowCapt	IAV Technologies	0–250 g m^{-2} s^{-1}	±5%	Open
Snow water equivalent (SWE)	SWE sensor (CS725)	Campbell Scientific	0–600 mm of water equivalent	±15 mm	Gap

[a] accuracy for daily totals.

forest malfunctioned soon after their deployment. With the proximity of the forest site to the gap site, ground temperature measurements from the gap station were therefore used for the analysis in the forest. Snow water equivalent (SWE) was only measured at the gap station at 6 hr intervals using a passive gamma SWE sensor (CS725). Two Hydroinnova SWE sensors (Hydroinnova, 2019) installed in the open and forest were

found to be not functioning well, and hence were not considered in the analysis. The precipitation radar sensor (WS700-UMB) was installed at a height of 10 m above the ground and all the other remaining sensors at a 2 m height.

The open site is equipped with two second-generation FlowCapt acoustic sensors to measure hourly blowing snow fluxes vertically integrated between 0–1 m and 1–2 m above the ground surface (Chritin et al., 1999; Cierco et al., 2007; Trouvilliez et al., 2015; IAV Technologies, 2019). A number of studies in the Swiss and French Alps (Lehning and Fierz, 2008; Naaim-Bouvet et al., 2010; Trouvilliez et al., 2015; Vionnet et al., 2018), the Indian Himalayas and Central Asia (Das et al., 2012; Zhang et al., 2022), the Arctic region (Jaedicke, 2001), and in Antarctica (Trouvilliez et al., 2014; Amory, 2020) have demonstrated the capability of the FlowCapt sensor to detect blowing snow. However, the accuracy of the FlowCapt sensor for quantitatively measuring the blowing snow fluxes has been debated in the literature (Cierco et al., 2007; Lehning and Fierz, 2008; Naaim-Bouvet et al., 2010; Trouvilliez et al., 2015). The second-generation sensor (used in this study) has significant improvements (Trouvilliez et al., 2015) overcoming many drawbacks of its first-generation counterpart (Cierco et al., 2007). Trouvilliez et al. (2015) found that the sensor still underestimates the snow fluxes quantities compared to a snow particle counter S7 sensor during a winter season in the French Alps, particularly during concurrent snowfall. However, they also showed its promising capability as a blowing snow event detector. Several other authors highlight the usefulness of the second-generation FlowCapt as a good aeolian snow transport event detector with a high level of confidence, together with its robustness to withstand hostile weather conditions for prolonged periods (e.g., polar environments), and its low power consumption (Trouvilliez et al., 2014; Amory, 2020).

3. Methods

The snowpack behavior at the three sites was examined from 01st December 2020– 15th April 2021 by computing the energy exchange components. Prior to calculating the energy budget components, all the raw measurements were inspected, and missing, and/or suspected erroneous values were screened, inventoried, and gap-filled accordingly. As such, no missing data were identified for the open and gap stations for the study period. Twenty isolated missing values were identified for the WS700-UMB measurements at the forest station and were filled with linear interpolation. Because of the robust filtering process based on quality number incorporated in the logger program, snow depth measurements were found to be reliable. However, despite that, one snow depth point at the open site was identified as completely out of trend (snow depth $>$ 2 m) and corrected with linear interpolation from the two neighboring time steps. Then, hourly measurements were directly used for the energy flux calculations at the open and forest stations. At the gap station, all data recorded in 15-minute time steps were aggregated to hourly averages (except for precipitation: hourly sum) and used for the energy flux calculations. Specific processing for the other meteorological variables and radiation fluxes are described in subsequent sections.

3.1. Data quality control and preprocessing

3.1.1. Radiation correction

Negative incoming and outgoing shortwave radiations during the night were set to zero. Corrections were made for snow covering and shading the upward-looking pyranometer sensor, specifically at the forest station where low winds were less efficient to clear the snow on the sensors. These periods were identified by available time-lapse photos and high albedo during daytime (>0.9). In such situations, the incoming radiation data were corrected by using an albedo for fresh snow ($\propto_{raw}$= 0.85; Oke (1987)) and multiplying it by the outgoing radiation (e.g., Conway et al., 2018; Hoelzle et al., 2022).

Additionally, solar radiation data were corrected for patchy snowpack conditions at the beginning and end of the study periods at all sites by considering the snow cover fraction within the sensor footprint. The snow cover fraction (SCF) was approximated as (Essery et al., 2013):

$$SCF = \min\left(1, \frac{snow\ depth}{d_0}\right) \quad (1)$$

d_0 was taken as 0.1 m in all sites. This value was decided by plotting daily raw albedo versus snow depth, which showed that albedo was influenced by exposed soil below 0.1 m of snow depth (Supplement Figure S1). The raw snow albedo ($\propto_{raw}$) was then corrected using the snow cover fraction.

$$\propto_{corr} = \frac{\propto_{raw} - (1 - SCF)\ \propto_{soil}}{SCF} \quad (2)$$

Where soil albedo ($\propto_{soil}$) was set to 0.15 based on snow-free observations in the fall. Then, the outgoing shortwave radiation was corrected by multiplying the incoming shortwave radiation by the corrected albedo ($\propto_{corr}$).

This correction was applied for 49, 46, and 34 days from the total of 135 days in the open, forest, and gap respectively.

A maximum value of 316 W m^{-2} was imposed on outgoing longwave radiation to avoid the bias from warmer snow-free soil in the sensor footprint (e.g., melting snow surface with a patchy snowpack). This maximum value was obtained by calculating outgoing longwave radiation (Q_{LWout}) for a snow surface temperature, T_s, of 273.15 K (0 °C) using Eq. (3) (Dewalle and Rango, 2008).

$$Q_{LWout} = \varepsilon\sigma\ T_s^4 + (1 - \varepsilon)Q_{LWin} \quad (3)$$

Where the emissivity ε is taken as 0.98 (Anderson, 1976), σ is the Stefan-Boltzmann constant (5.67 $\times$ 10^{-8} W m^{-2} K^{-4}), and Q_{LWin} is the incoming longwave radiation.

3.1.2. Local precipitation data preparation

In a recent study at the gap station, Paquotte and Baraer (2021) used precipitation data from the Pierre-Elliott-Trudeau station (YUL), situated 40 km east of the study site (Environment and Climate Change Canada, 2021) reasoning that it is situated in the same precipitation corridor as Sainte-Marthe, and in a similar physiographic context. The authors used the data from November 2018 to April 2019, before the deployment of the WS700-UMB sensor at the site. We compared the total cumulative precipitation of the WS700-UMB with YUL for the 2020–2021 winter season which showed that they are in the same order of magnitude (Supplement Figure S2). Therefore, the local precipitation data from the WS700-UMB measurements at the gap station was used for all three sites in this study. However, since the automatic separation of the precipitation into rainfall and snowfall by the WS700-UMB sensor appeared to be erroneous, the precipitation phase separation was done by adopting a 2 °C temperature threshold based on the mean winter relative humidity of 90% during the precipitation events at the site (Jennings et al., 2018b).

3.1.3. Calculation of mean snowpack temperature

The mean snowpack temperature was obtained by averaging the four thermistor measurements within the snowpack when the snow depth was higher than 35 cm. When snow depth was below 35 cm, only the thermistors located 5 cm or more below the snow surface were used for averaging, in order to avoid direct solar radiation effects on thermistors.

3.1.4. Calculation of specific humidity

The specific humidity, q, was calculated from the relative humidity measurements at each site (Armstrong and Brun, 2008).

$$q = 0.622\ RH\ \rho_w/(\rho_a - \rho_w) \quad (4)$$

Where RH is the relative humidity as a factor, ρ_w is the density of

water vapor (kg m^{-3}), and ρ_a is the density of air (kg m^{-3}).

3.2. Calculation of surface energy balance

The energy balance for the snowpack (Fig. 2) was calculated at an hourly time step, using Eq. (5) (adapted from Dewalle and Rango (2008)).

$$Q_M + \frac{dU}{dt} = Q_{SW} + Q_{LW} + Q_S + Q_L + Q_R + Q_{SF} + Q_G \quad (5)$$

Where Q_M is the heat available for melt, U is the internal energy of the snowpack, Q_{SW} is the net shortwave radiation heat flux, Q_{LW} is the net longwave radiation heat flux, Q_S is the sensible heat flux, and Q_L is the latent heat flux caused by evaporation, sublimation, or condensation. Q_R is the sensible and latent heat flux associated with rain-on-snow events, Q_{SF} is the sensible heat associated with solid precipitation (snowfall), and Q_G is the heat exchange at the snow-ground interface. All fluxes on the right side of the energy balance equation, except Q_S and Q_L, were derived from the raw measurements collected at the respective weather station at each site. Q_{SW} and Q_{LW} were measured directly at each site using CNR4 sensors (Table 1) and were corrected as described in Sections 3.1.1. $Q_M + \frac{dU}{dt}$ was solved as the residual of the other energy fluxes as depicted in Eq. (5). All energy terms are expressed in W m^{-2} and are positive when received by the snowpack and negative when lost by the snowpack. The analysis was calculated from December 2020 to April 2021. All energy fluxes were calculated at hourly time steps and then averaged to daily values. Then, the daily surface energy fluxes calculated for days with snow depths less than 5 cm (i.e., snow cover fraction less than 0.5) were omitted because of the high uncertainty involved with a very thin snowpack. Mean weekly values were then calculated from daily values to simplify the presentation and interpretation of the results. Mean weekly values were calculated when at least five days of a week had snow depths equal or higher than 5 cm.

3.2.1. Turbulent sensible and latent heat flux

The turbulent fluxes were calculated using the bulk aerodynamic method (Price and Dunne, 1976; Oke, 1987).

$$Q_S = \rho_a c_p C_h u_a (T_a - T_s) \quad (6)$$

$$Q_L = 0.622\ \rho_a L C_e u_a (e_a - e_s)/P_a \quad (7)$$

Where ρ_a is the density of air (kg m^{-3}), c_p is the specific heat of air at constant pressure (1005 J kg^{-1} K^{-1}), C_h is the bulk exchange coefficient for the sensible heat flux (unitless), u_a is the wind speed (m s^{-1}), T_a is the air temperature (K), T_s is the snow surface temperature (K), L is the latent heat of vaporization (2.501×10^6 J kg^{-1}) when $T_s = 0$ °C or sublimation (2.835×10^6 J kg^{-1}) when $T_s < 0$ °C, C_e is the bulk exchange coefficient for the latent heat flux (unitless), e_a is the atmospheric vapor pressure (Pa), e_s is the vapor pressure at the snow surface (Pa), and P_a is the atmospheric pressure (Pa). T_s was measured using the outgoing (Q_{LWout}) and incoming (Q_{LWin}) longwave radiation measurements and rearranging the longwave radiation balance in Eq. (3) (Helgason and Pomeroy, 2012a; Steiner et al., 2018).

The bulk exchange coefficients for sensible and latent heat under neutral atmospheric conditions, C_n, was estimated using Eq. (8) (Conway and Cullen, 2013).

$$C_n = \frac{k^2}{[ln(z_a/z_0)]^2} \quad (8)$$

Where the von Karman constant k is 0.4, z_a is the height of the wind measurement from the snow surface in meters and z_0 is the snow roughness that was assumed to be at 0.0005 m, which is similar to that used by Paquotte and Baraer (2021) in the same study area. In situations of non-neutral atmospheric conditions, C_n should be corrected according to the relevant atmospheric stability to obtain C_h and C_e. Atmospheric stability can generally be assessed by the bulk Richardson number, R_{iB} (Oke, 1987).

$$R_{iB} = g\ z_a (T_a - T_s)/T_m u_a^2 \quad (9)$$

Where g is the acceleration of gravity (9.8 m s^{-2}) and T_m is $(T_a + T_s)/2$. While the conventional approach involves the use of virtual potential temperature, standard temperature is often used, as here, as the difference is negligible within a thin air layer (Monin and Yaglom, 1971).

If the conditions are stable ($R_{iB} > 0$), the bulk exchange coefficient is (Price and Dunne, 1976; Boike et al., 2003):

$$C_e = C_h = \frac{C_n}{(1 + 10R_{iB})} \quad (10)$$

and for unstable conditions:

$$C_e = C_h = C_n\ (1 - 10R_{iB}) \quad (11)$$

A minimum of 0.3 m s^{-1} was imposed on u_a to avoid suppressing turbulent fluxes completely at low wind speeds (Martin and Lejeune, 1998; Conway and Cullen, 2013). In addition, a sensitivity analysis was carried out for the turbulent flux calculation using four different wind threshold values, a windless coefficient, and two other stability correction methods to check the sensitivity of the residual energy balance, $Q_M + \frac{dU}{dt}$, to the different calculation methods (Supplement Table S1 and Figure S3). Error statistics for the different methods did not vary considerably, except when including a windless coefficient (Supplement Table S2 and S3).

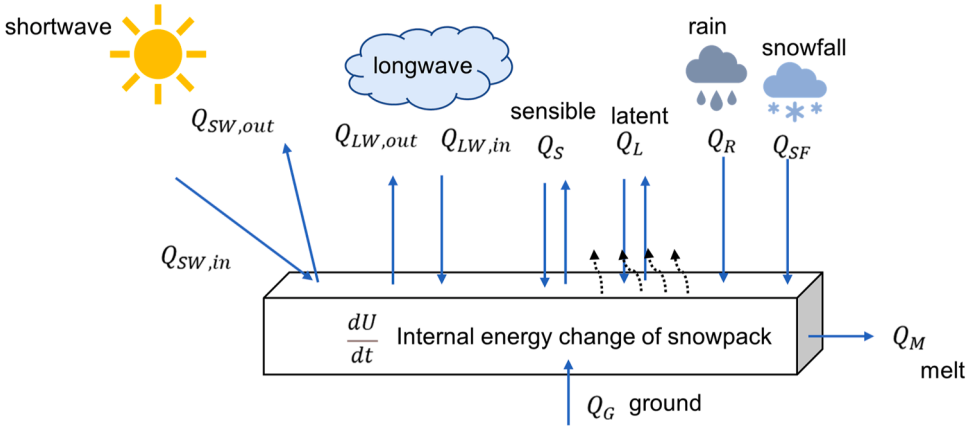

Fig. 2. Schematic illustration of snowpack energy balance components.

3.2.2. Precipitation energy flux

Heat flux due to rain-on-snow was calculated in two stages (Dewalle and Rango, 2008) as:

$$Q_R = Q_{r1} + Q_{r2} \tag{12}$$

The first source of energy input by rain is the sensible heat brought to the snow surface and used to bring it to the freezing point, 0 °C:

$$Q_{r1} = P_r c_w \rho_w (T_r - 0) \tag{13}$$

Where P_r is the rainfall intensity (m s^{-1}), c_w is the specific heat of liquid water (4187 J kg^{-1}°C^{-1}), ρ_w is the density of liquid water (1000 kg m^{-3}), T_r is the temperature of rain (°C), which is assumed to be equal to T_a in this study.

The second source of energy input is the release of latent heat of fusion when rain freezes on a subfreezing snowpack (< 0 °C).

$$Q_{r2} = P_r \rho_w L_f \tag{14}$$

Where L_f is the latent heat of fusion (0.334 × 10^6 J kg^{-1}).

The sensible heat flux advected by snowfall was calculated as:

$$Q_{SF} = P_{SF} c_i \rho_w (T_{SF} - 0) \tag{15}$$

Where P_{SF} is the snowfall intensity (m s^{-1}), c_i is the specific heat of ice (2100 J kg^{-1} °C^{-1}), ρ_w is the density of liquid water (1000 kg m^{-3}), T_{SF} is the temperature of snowfall (°C), which is assumed here to be equal to T_a.

3.2.3. Ground heat flux

The ground heat conduction to the base of the snowpack was be computed as (Dewalle and Rango, 2008):

$$Q_g = k_g \frac{dT_g}{dz} \approx \frac{k_g (T_{10} - T_0)}{\frac{10}{100}} \tag{16}$$

Where k_g denotes the thermal conductivity of soil (W m^{-1}°C^{-1}), T_{10} is the temperature measured 10 cm below the ground surface, and T_0 is the temperature measured at the ground surface (base of the snowpack). We used the temperature gradient between the base of the snowpack and the 10 cm depth ($\frac{dT_g}{dz}$, °C m^{-1}) for the ground heat calculation, as it was observed from the measurements that the ground temperature did not fluctuate much below 10 cm. k_g generally varies with the moisture and organic matter content of the soil, typically between 0.2 and 2.2 W m^{-1}°C^{-1} (Oke, 1987). In this study, k_g was calculated using the porosity (φ) of the soil at each site. The maximum measured volumetric water content in the spring was used to estimate the soil porosity, assuming the pores were saturated by the beginning of spring with snowmelt. Then, by taking a typical thermal conductivity of the dry soil (k_{dry}) for each site (Oke, 1987) and ice ($k_{ice} = 2.24$), k_g is given by:

$$k_g = k_{dry}(1 - \varphi) + k_{ice}\varphi \tag{17}$$

Table 2 shows the k_g values obtained using respective φ and k_{dry} values at each site. Soil types at each site were obtained from the Institute for Agri-Environments (IRDA).

3.2.4. Residual energy flux

The residual energy flux, or net energy balance, is a combination of melt energy (Q_M) and change of internal energy (cold content) of the snowpack ($\frac{dU}{dt}$). Q_M is equal to 0 when the right hand side of the energy balance equation (Eq. (5)) is negative (snowpack cooling). Otherwise, $Q_M + \frac{dU}{dt}$ is equal to the right member of the energy balance equation, whose value represents the maximum melt estimate if the snowpack is isothermal. As such, snowpack melting occurs when the available energy is large enough to eliminate the cold content and induce melt, else only warming of the snowpack occurs. $\frac{dU}{dt}$ was not calculated separately in this study due to the absence of continuous snow pit or SWE measurements and the high uncertainty involved with the calculation process (Dewalle and Rango, 2008; Helgason and Pomeroy, 2012a; Jennings et al., 2018a). More often, $\frac{dU}{dt}$ is modeled with a multilayer snowpack assumption (Helgason and Pomeroy, 2012a; Conway et al., 2018; Jennings et al., 2018a; Parajuli et al., 2021). However, by keeping $\frac{dU}{dt}$ at the left side of Eq. (5), we are still able to explain the different snowpack behaviors observed at each site by the changes of the right members of the energy balance equation.

Table 2
Soil types, parameters, and thermal conductivity of soil (k_g) at each site.

	Open	Gap	Forest
Soil type	Clay	Sandy loam	Sandy loam
φ	0.40	0.45	0.45
k_{dry} (W m^{-1}°C^{-1})	0.25	0.30	0.30
k_g (W m^{-1}°C^{-1})	1.05	1.17	1.17

3.3. Analysis of measured meteorological variables and snow energy balance components

Changes in measured meteorological variables and weekly snow energy fluxes between the three sites were analysed in three distinct periods based on the daily evolution of the snow depth during the study period: a first "Early winter period" from December to mid-January when the snowpack is thin (<10 cm) and transient, a second "Accumulation period" from mid-January to February 28th (starting date of ablation) when the snowpack is thickening, and a third "Ablation period" from February 28th onward with sustained ablation of the snowpack (see Fig. 3). In addition to the weekly changes, the percentage contribution of each energy flux for the total energy balance during the three periods were examined and compared between the three sites. The individual flux contribution was calculated by dividing the absolute value of the energy flux by the sum of the absolute value of all the energy fluxes. In order to identify the energy components that control the snowpack cooling or warming and melting (i.e., net energy balance in our study) at each site, The Spearman partial correlation coefficient between each energy term and the residual energy flux, or net energy balance ($Q_M + \frac{dU}{dt}$), was calculated for the three periods. As such, while the highest percentage contribution of an energy term to the total energy balance is noteworthy, it does not necessarily imply that it has the most significant influence on snowpack cooling or warming (Kinnard et al., 2022).

3.4. Blowing snow analysis at open site

Mean hourly blowing snow fluxes measured by the two FlowCapt sensors (measurements along the height 0–1 m and 1–2 m) were summed and analyzed from mid-January 2021 to March 2021 when a stable snow cover was present and before significant snowmelt began at the study site (Accumulation period in Fig. 3). For the analysis, snow flux measurements higher than the lower detection limit of the FlowCapt (0.002 g m^{-2} s^{-1} considering both sensors) were considered as blowing snow events. First, we examined and analyzed the relationships between blowing snow measurements and meteorological conditions using bivariate relationships. As such, blowing snow events with and without concurrent snowfall were compared against hourly meteorological measurements such as wind speed, air temperature, and relative humidity. Then, we examined the weather conditions associated with the blowing snow events and the thermodynamic feedback effects of blowing snow on energy balance in the open under snowfall-free conditions. The former was investigated by comparing median differences of relative humidity, air temperature, atmospheric pressure, wind speed, and wind direction between blowing snow and no-blowing snow events in the open. The latter was achieved by comparing median differences and quantifying the changes in energy fluxes and associated meteorological parameters between the open and gap sites during blowing snow

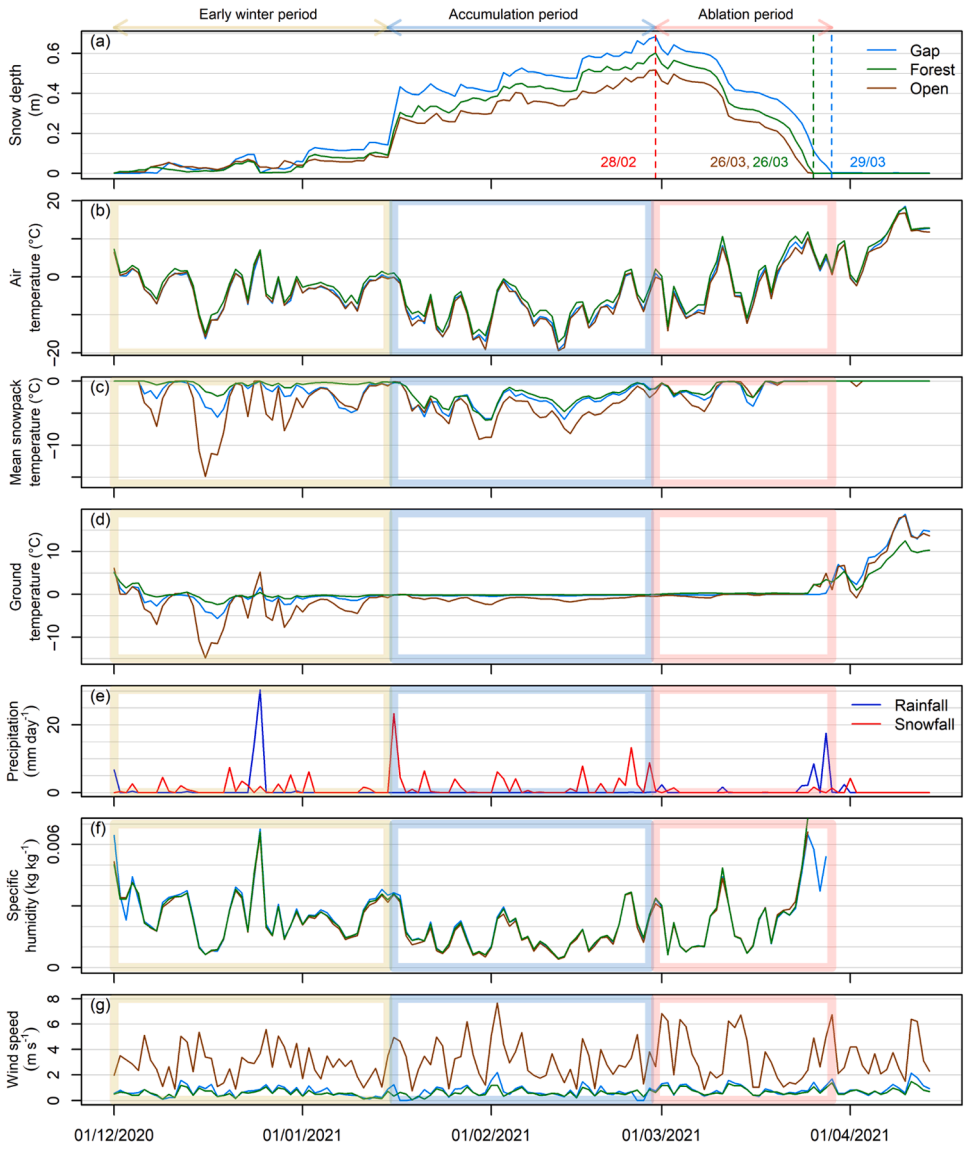

Fig. 3. Meteorological conditions and snowpack characteristics at the three study sites during winter 2020–2021 with a) daily snow depth, with the start (red) and end (brown, blue, green) of the ablation period indicated by stippled vertical lines and corresponding dates; b) daily air temperature; c) daily mean snowpack temperature; d) daily ground (snowpack base) temperature; e) snowfall and rainfall; f) specific humidity; and g) wind speed. Early winter, accumulation, and ablation periods are demarcated by yellow, blue, and red colors and are further explained in the text.

and no-blowing snow time steps recorded by the FlowCapt. Given the proximity of the sites, the weather conditions triggering blowing snow fluxes would affect similarly all the sites; hence, differences between open and gap are expected to reflect the feedback effect of blowing snow on energy fluxes and associated meteorological variables. The median was used as estimator of central tendency due to the non-normal distributions of the meteorological and energy-balance variables. Accordingly, the nonparametric Wilcoxon rank-sum test (Wilcoxon, 1945) was used to test the significance of the difference in meteorological and energy balance variables between blowing and no-blowing snow events. In addition to latent and sensible heat feedbacks, radiative feedbacks were also investigated for incoming longwave radiation but not for incoming shortwave radiation, as the reference gap site is largely shaded by surrounding trees which precludes meaningful comparisons with the open site using hourly data. Absolute (*AE*) and relative (*RE*) effect metrics are introduced to quantify the feedback effects of blowing snow. *AE* shows the absolute influence of blowing snow on individual fluxes or meteorological variable, i.e., in their original units, while *RE* allows to compare the relative feedback effects between the different variables, i. e., on a common scale. Since the data is deviates from normality and to avoid bias from outliers, median values of the variables were used instead of mean when calculating the absolute and relative effects.

$$AE = med(open - gap)_{BS} - med(open - gap)_{No\ BS} \quad (18)$$

Where $med(open - gap)_{BS}$ indicates the median difference between open and gap measurements during blowing snow periods and $med(open - gap)_{No\ BS}$ indicates the median difference between open and gap measurements during no-blowing snow periods. *AE* should be near zero if blowing snow has no thermodynamic impacts at the open site.

$$RE = (AE\ /\ (med(open_{BS}) - AE)) * 100 \quad (19)$$

Where $med(open_{BS})$ indicates the median of observed meteorological variable or energy flux during blowing snow periods.

4. Results

4.1. Measured meteorological variables

During the observation period, the highest maximum snow depth of 0.68 m was found in the gap, and the lowest maximum snow depth of 0.52 m was found in the open site, with an intermediate snow depth of 0.60 m being found in the forest site (Fig. 3a). Similarly, the highest average snow depth was observed in the gap (0.27 m), lowest in the open (0.19 m), and intermediate in the forest (0.22 m). The snowpack disappeared on the same date (26/03/2021) in the open and forest and lasted longer in the gap (29/03/2021). High air temperature throughout the winter at the forest site compared to the gap and open sites indicates a comparatively warmer climate in the forest (Fig. 3b). The mean air temperature was –3.3°C at the open site, –3.0 °C in the gap, and –1.9 °C in the forest throughout the observation period. The mean snowpack temperature shows a substantial variation in the open compared to the forest and gap (Fig. 3c). The snowpack at the open site was the coldest among the sites, the forest snowpack the warmest, and the gap snowpack falling in between. Similarly, the ground surface (snowpack base) temperature was colder and more variable at the open site, compared to the forest site while the gap showed an intermediate behavior (Fig. 3d). The ground surface temperature at the forest and gap sites displayed freezing events in early winter, while a prolonged zero-curtain effect (near-zero temperature) is observed during the accumulation and ablation period. The open site stands out with a near-continuous frozen state throughout winter. Significant rainfall events are observed in the early winter and ablation periods, but not in the accumulation period (Fig. 3e). Specific humidity did not vary much between the sites indicating almost similar moisture contents in all the sites (Fig. 3f). Wind speed was substantially higher in the open compared to forest and gap. Being sheltered by trees, the forest shows the lowest wind speeds during the study period (Fig. 3g).

With the absence of SWE data, snowpack evolution was analyzed using the changes in snow depth. Daily snow depth reduction rates (i.e., decrease of snow depths between two consecutive days) estimated using the measured snow depths during the ablation period were used to compare the snowpack evolution between the sites (Fig. 4). Despite having a considerable difference in snow depths (Fig. 3a), almost similar snow depth reduction rates were observed between the sites (Fig. 4).

4.2. Energy balance components

The weekly energy flux components and associated mean energy fluxes are portrayed in Fig. 5 for the early winter, accumulation, and ablation periods between the sites. Fig. 6 (also in Supplement Table S4) illustrates the mean energy fluxes and the percentage contribution of each energy flux to the total energy balance during the aforementioned three periods between the sites. The partial correlation coefficient values between energy terms and the residual energy flux, or net energy balance ($Q_M + \frac{dU}{dt}$) for the three periods are shown in Fig. 7 (also in Supplement Table S5). In Fig. 5, the energy balance components were plotted by moving all the energy terms to the right side of Eq. (5), so that the sum of all terms is zero. In other words, when the right-hand side of Eq. (5) is negative, the plotted $Q_M + \frac{dU}{dt}$ (grey color bar) is positive and vice versa. Therefore, in Fig. 5, a positive $Q_M + \frac{dU}{dt}$ indicates the accumulation of a cold content (heat loss) in the snowpack. Conversely, a negative $Q_M + \frac{dU}{dt}$ indicates an energy surplus and snowmelt, except at subfreezing temperatures, then the excess energy should indicate a warming of the snowpack.

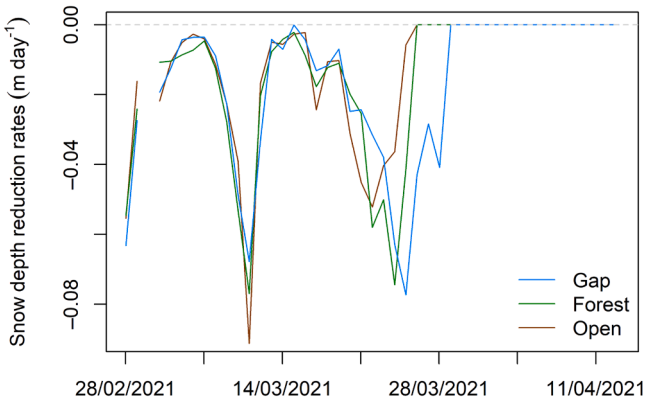

Fig. 4. Snow depth reduction rates in the three sites.

4.2.1. Early winter period

Throughout the early winter period, net longwave radiation was the most important energy flux in open and gap sites, with an average contribution of 38.5% and 48.3% at the open and gap respectively (Fig. 6 and Supplement Table S4). Sensible heat fluxes were always positive except for week 2, during which it was slightly negative at the open. Latent heat fluxes were always negative at all sites. Snowpacks at all sites received a negligible amount of energy from rainfall, except during week 1 as a result of the 30 mm rainfall event that occurred in the early winter period (see Fig. 3e). Energy advected due to snowfall was negligible at all sites. Nevertheless, the most striking difference in energy fluxes during the early winter period compared to the later periods is the significant ground heat fluxes at all sites (4.7–24.9%), though more pronounced at the open and gap (Fig. 5 and 6). The net energy balance at all sites was generally negative (positive grey bar in Fig. 5), hence reflecting cooling of the snowpack. The highest partial correlation coefficient between individual fluxes and the net energy balance at all sites was for net longwave radiation (Fig. 7a). This indicates that the most significant control of the net energy balance came from longwave radiation. However, the application of the energy balance equation in the early winter period when the snowpack is thin (less than 10 cm), comes with some limitations and a higher degree of uncertainty, which will be commented in the discussion section.

4.2.2. Accumulation period

Net radiation (both shortwave and longwave components) was the most important energy balance component at all sites, while turbulent fluxes (sensible and latent components) were only substantial at the open site (Fig. 5 and 6). During the study period, the net radiation component accounted for 68.1%, 87.5%, and 56.8% of the total energy budget in the open, gap, and forest respectively (Fig. 6d–f). Turbulent flux contributions to the energy budget were 23.7%, 6.5%, and 8.9% in the open, gap, and forest respectively. Net radiation was negative at the open and gap, but positive in the forest (both weekly and on average). As seen in Fig. 5, negative net radiations at open and gap were often associated with smaller positive net shortwave and larger negative net longwave radiations throughout the accumulation period whereas, at the forest, positive net radiations were associated with slightly larger net shortwave radiations and smaller negative or sometimes even positive (in weeks 6 and 9) net longwave radiations. At all sites, although more prominent at open, sensible heat fluxes were always positive, and latent heat fluxes always negative. The ground heat flux and the energy advected by precipitation (both rainfall and snowfall) were negligible throughout the accumulation period. The net energy balance was negative (positive grey bar in Fig. 5) throughout the accumulation period at the open and gap indicating cooling of the snowpack, but became positive during the last two weeks of the period (weeks 9 and 10). In contrast, the net energy balance was slightly positive (negative grey bar in Fig. 5) throughout the accumulation period in the forest, indicating warming/and or melting of the snowpack. Similar to the early winter period, the net longwave radiation exerted the greatest control on the net energy balance (Fig. 7b).

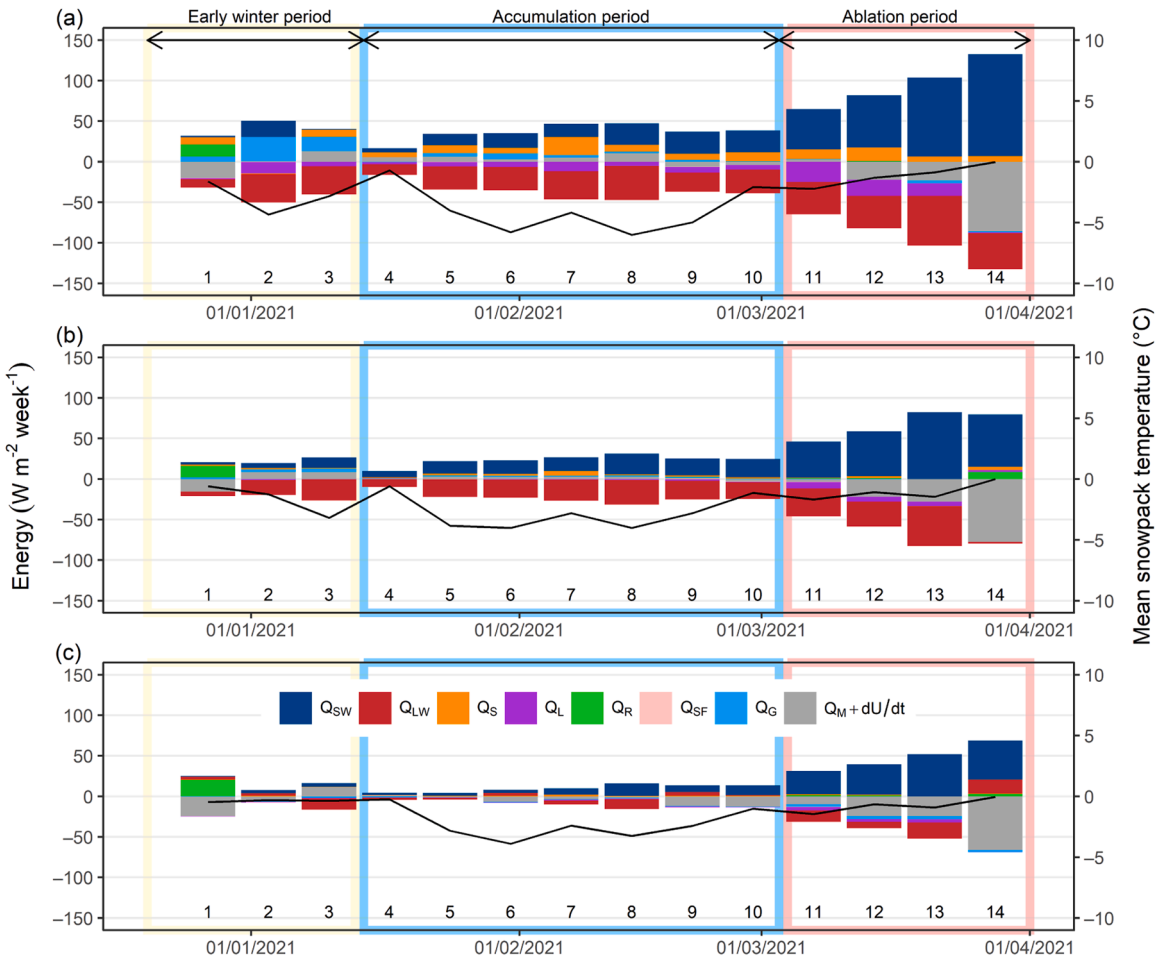

Fig. 5. Mean weekly energy fluxes and mean snowpack temperatures (black lines) at the three study sites: a) open; b) gap; and c) forest. Q_{SW}: Net shortwave radiation, Q_{LW}: Net longwave radiation, Q_S: Sensible heat flux, Q_L: Latent heat flux, Q_R: Rainfall energy flux, Q_{SF}: Snowfall energy flux, Q_G: Ground heat flux, and Q_M+dU/dt: Net energy balance. Negative net energy balance (grey bar) implies warming and melting of the snowpack whereas a positive net energy balance indicates cold content accumulation and cooling of the snowpack.

4.2.3. *Ablation period*

The transition from the accumulation to the ablation period was accompanied by a clear increase in net shortwave radiation at all sites (Fig. 5 and 6). Net radiation remained positive throughout the ablation period. Sensible heat fluxes were still positive, indicating an energy source for snowpacks at all sites. There was an increase in latent heat fluxes during the ablation period at all sites. However, net radiation still had the highest contribution to the total energy budget (68.9% at open, 68.8% at gap, and 54.6% at forest). There was negligible ground heat flux and energy advected by precipitation (both rainfall and snowfall) at all sites. However, the forest snowpack shows a comparatively higher ground heat transfer from the snowpack base to the ground compared to the other two sites throughout the ablation period (Fig. 5c and 6c). The net energy balance was generally positive (negative grey bars in Fig. 5) at all sites, indicating a warm and melting snowpack. In the forest, net longwave radiation also contributed to snowmelt, apart from net shortwave radiation in week 14. However, latent heat fluxes had the greatest control over the net energy balance at the sites, except in the forest, where shortwave radiation correlated slightly better with the net energy balance (Fig. 7c).

4.3. *Blowing snow*

Hourly blowing snow measurements varied from 0.002 to 8.6 g m^{-2} s^{-1} in the accumulation period (presented on a log-scale for better interpretability in Fig. 8). Most events with concurrent snowfall had higher intensity fluxes (Fig. 8a–c) while most events under snowfall-free conditions are clustered in low-intensity snow fluxes, except for a few events (Fig. 8d–f). Irrespective of snowfall or snowfall-free conditions, the intensity of blowing snow fluxes increases with increasing wind speeds (Fig. 8a and d). The relationship is more linear for snowfall events (Fig. 8a), which may reflect the fact that a large part of the blown snow comes from snowfall, whose flux would increase proportionally with wind speed. In contrast, under snowfall free conditions, higher fluxes only begin above wind speeds of 4 m s^{-1}. No simple relationships emerge between blowing snow fluxes and air temperature and humidity. However most blowing snow events, especially the high-intensity ones, appear to occur between –10 °C and 0 °C (Fig. 8b and e), and 70–100% of relative humidity (Fig. 8c and f). Of all the hourly blowing snow events, 75% occurred during snowfall-free conditions. Blowing snow with concurrent snowfall does not show a clear trend towards either increase (deposition) or decrease (erosion) in snow depth measured by the ultrasonic snow depth sensor (SR50) (Fig. 8a–c). However, deposition (increasing snow depth) predominated over erosion for high-intensity blowing snow fluxes under snowfall-free conditions (blue colored high-intensity blowing snow fluxes in Fig. 8d–f and Supplement Figure S4). As such, at the end of the study period, snow depth showed a net gain of 0.16 m (total gain of 0.99 m and total loss of 0.83 m) at the AWS location (point scale) due to blowing snow fluxes under snowfall-free conditions. This corresponds to 29% of the maximum hourly snow depth of 0.55 m recorded during the study period.

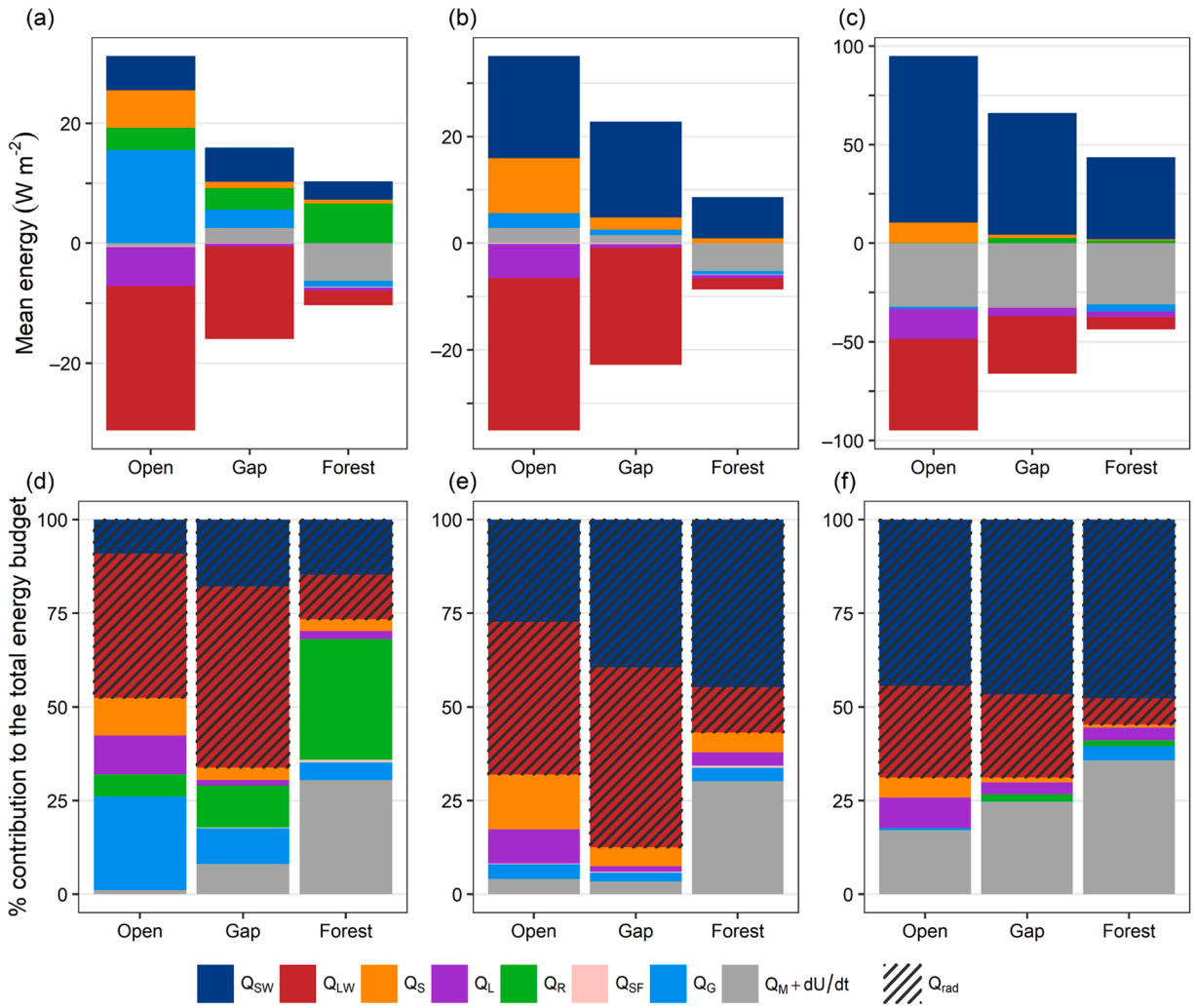

Fig. 6. Mean energy balance components (top row) and their contribution (%) to the total energy budget (bottom row) in a, d) early winter period; b, e) accumulation period; and c, f) ablation period. Q_{SW}: Net shortwave radiation, Q_{LW}: Net longwave radiation, Q_S: Sensible heat flux, Q_L: Latent heat flux, Q_R: Rainfall energy flux, Q_{SF}: Snowfall energy flux, Q_G: Ground heat flux, Q_M+dU/dt: Net energy balance, and Q_{rad}: Net radiation (Q_{SW}+ Q_{LW}).

4.3.1. *Weather conditions associated with blowing snow events*

Blowing snow fluxes under snowfall-free conditions occurred during periods with colder air temperature and lower relative humidity (Fig. 9a, b), and higher atmospheric pressure and wind speed (Fig. 9c, d) compared to periods with no-blowing snow fluxes. Wind directions were generally similar in both scenarios, i.e., predominantly from the West (Fig. 9e).

4.3.2. *Feedback effects of blowing snow on energy balance*

Nonparametric Wilcoxon rank-sum test showed that the difference between no-blowing snow (No BS) and blowing snow (BS) were statistically significant (p values < 0.05), reflecting the feedback effects of blowing snow on meteorological variables and energy fluxes in the open site. Compared to no-blowing snow periods, blowing snow periods under snowfall-free conditions show higher snowpack latent heat losses (more negative Q_L, Fig. 10a), lower sensible heat gains (less positive Q_S, Fig. 10b), and a decrease in incoming longwave radiation (Q_{Lwin}, Fig. 10c). Increased relative humidity (Fig. 10d) and air vapor pressure (e_a, Fig. 10e), a cooling of air temperature (T_a, Fig. 10f), an increase in wind speed (Fig. 10g), and a decrease in vapor pressure difference (e_a-e_s, Fig. 10h) and temperature difference (T_a-T_s, Fig. 10i) are also observed in the open relative to gap. Both latent and sensible heat fluxes are higher in the open than in the gap and are on average negative and positive, respectively (Fig. 5, 6, and Supplement Figure S5). Hence, the more negative Δ latent heat flux and decrease in Δ sensible heat flux in Fig. 10 suggest that latent heat losses are accentuated, and sensible heat gains attenuated, in the open during blowing snow periods. On average, incoming longwave radiation, relative humidity, and air vapor pressure are higher in the gap than that in open (Supplement Figure S5 and negative medians in Fig. 10c, d, and e). Therefore, the more negative Δ incoming longwave radiation indicates reduced incoming longwave radiation in the open during blowing snow events. Similarly, the less negative Δ relative humidity and Δ air vapor pressure suggest that blowing snow results in an increase in relative humidity and air vapor pressure in the open. This increase in vapor pressure is driving a reduction of the vapor pressure difference between the air and snowpack (i.e., less negative e_a-e_s). The vapor pressure difference is mostly positive in the gap and negative in the open (Supplement Figure S5). While air temperature is slightly cooler in the open than in the gap during no-blowing snow conditions (Supplement Figure S5), this difference accentuates during blowing snow, indicating a cooling effect of blowing snow in the open. The temperature difference between the air and snowpack is mostly positive in open and gap (thereby driving positive sensible heat fluxes, Supplement Figure S5). Hence the cooling effect of blowing snow results in a reduced positive temperature gradient in the open. The increase in Δ wind speed shows that wind speeds increase more in the open than at the gap during blowing snow events, due to the sheltered conditions at the gap (Fig. 3g and Supplement Figure S5).

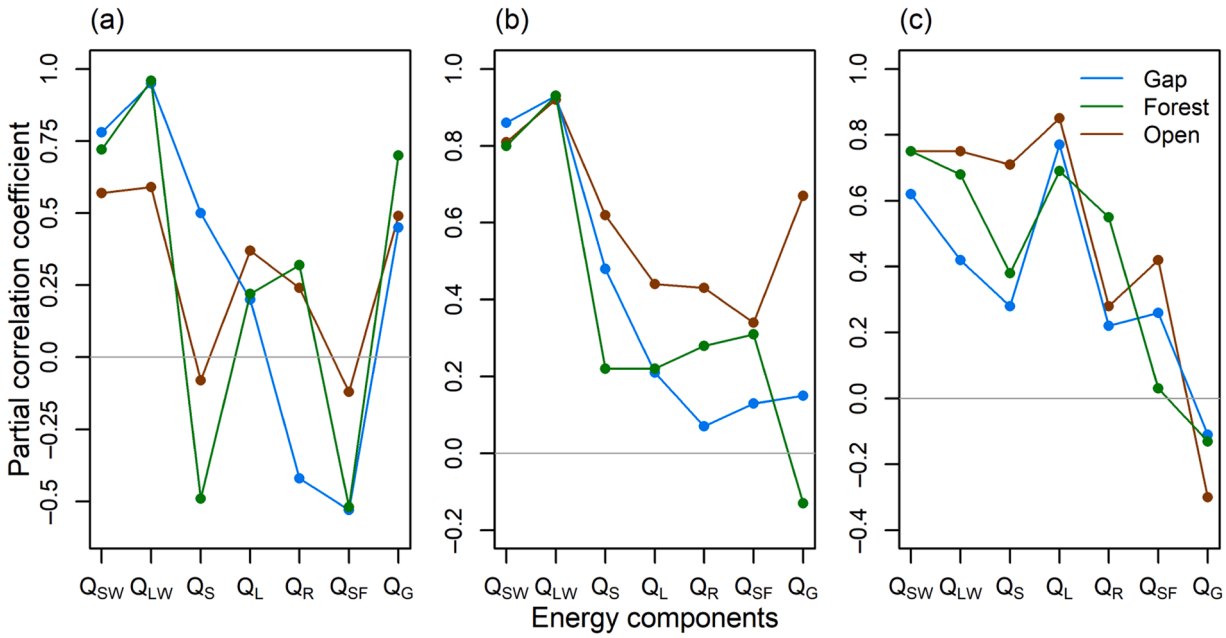

Fig. 7. Partial correlation coefficients between individual energy terms and net energy balance (Q_M+dU/dt): a) early winter period; b) accumulation period; and c) ablation period.

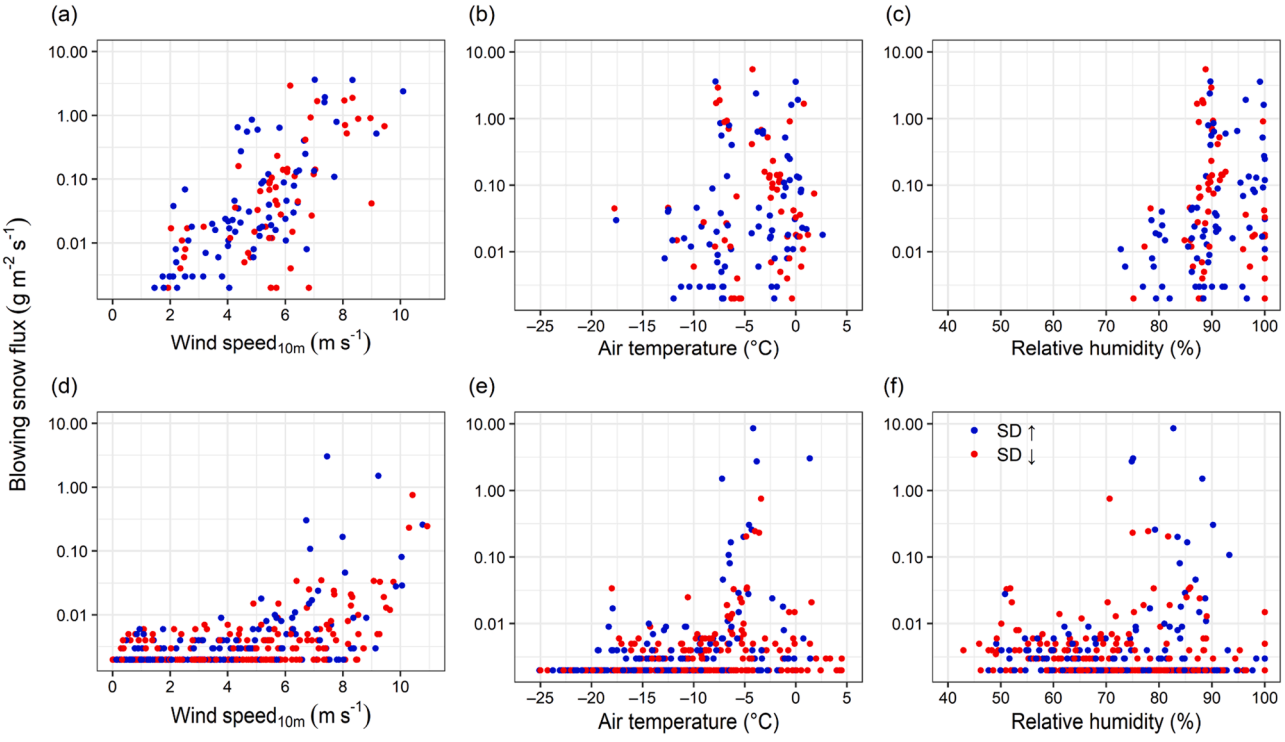

Fig. 8. Relationship between hourly blowing snow fluxes and meteorological conditions. Blue (red) dots indicate events with an increase (decrease) in snow depth recorded by SR50. Top row: events with concurrent snowfall; bottom row; snowfall-free conditions. a, d) wind speed at 10 m height from the snow surface (extrapolated using wind logarithmic profile); b, e) air temperature; and c, f) relative humidity. All y-axes are displayed in log scale for better visibility of the data distribution.

To discard the effect of the notable different wind regimes between the open and gap on latent and sensible heat fluxes, the latent and sensible heat fluxes at the gap were recalculated using wind speed at the open. Under the same wind regime, and despite the reduced vapor pressure gradient (Fig. 10h) the latent fluxes were still slightly greater (more negative) in the open during blowing snow periods compared to no-blowing snow periods, but the difference is not statistically significant (Fig. 11a). The sensible heat gains were still lower during blowing snow (Fig. 11b, Supplement Figure S6), in accordance with the reduced positive temperature gradient in the open (Fig. 10i). To further investigate the other possible causes for the altered latent and sensible heat fluxes during blowing snow, we also compared changes in air stability

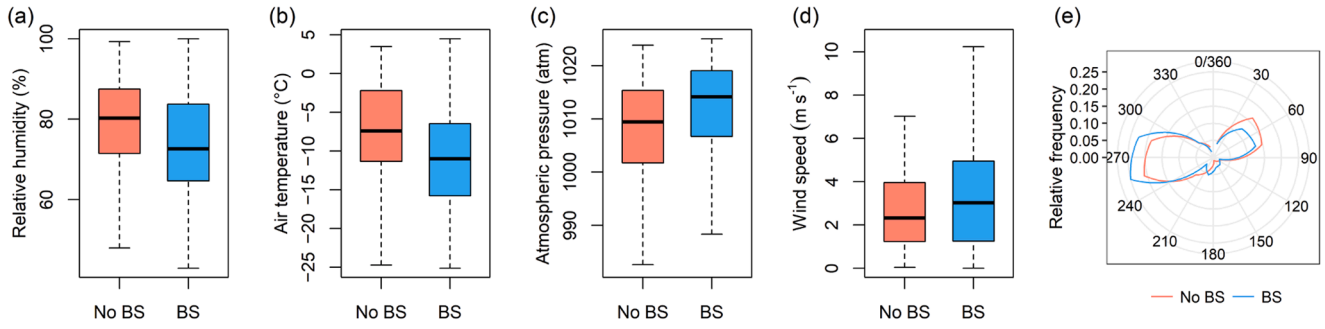

Fig. 9. Meteorological conditions during no-blowing snow (red) versus blowing snow (blue) under snowfall-free conditions. a) relative humidity; b) air temperature; c) atmospheric pressure; d) wind speed; and e) relative frequency of wind direction in 30-degree bins.

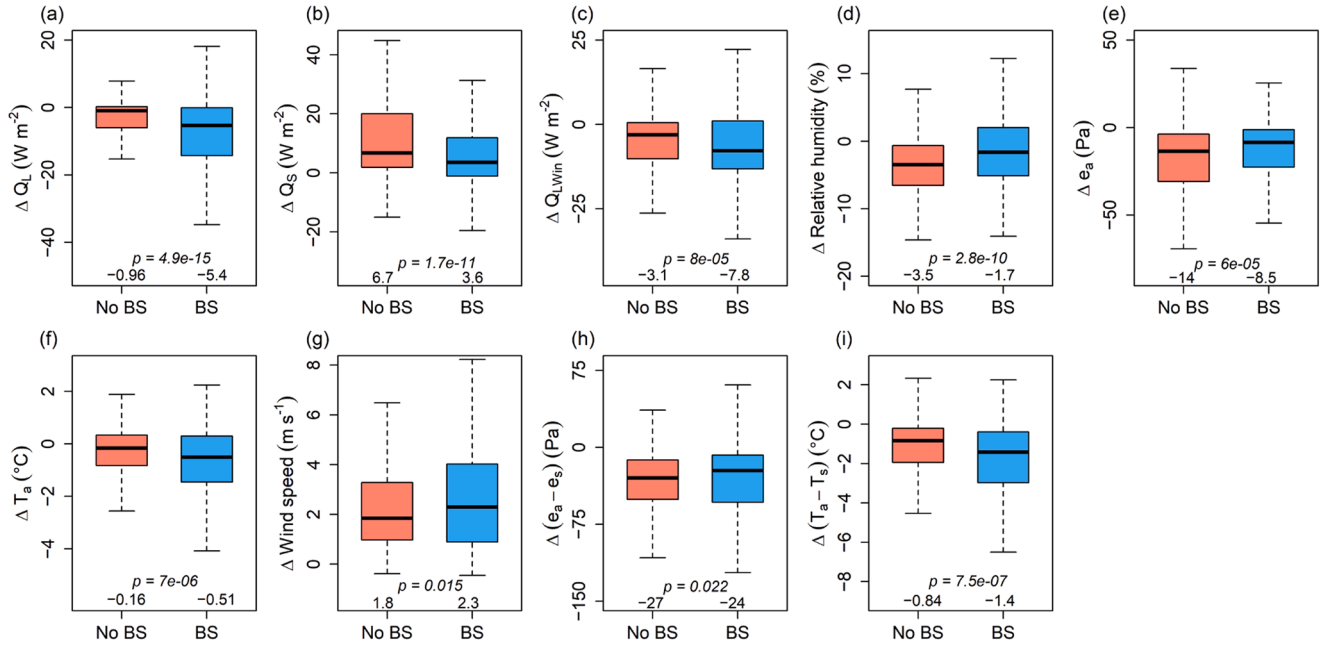

Fig. 10. Feedback effects of blowing snow in terms of the difference between open and gap in a) latent heat flux; b) sensible heat flux; c) incoming longwave radiation; d) relative humidity; e) air vapor pressure; f) air temperature; g) wind speed; h) vapor pressure difference between air and snowpack surface; and i) temperature difference between air and snowpack surface. Median differences (in regular font) and *p* values (in italic) from Wilcoxon rank-sum test are reported in each panel.

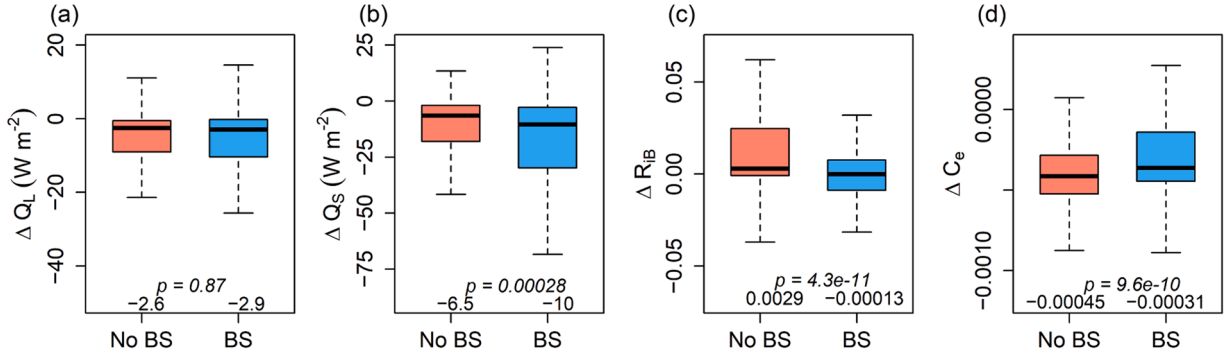

Fig. 11. Under open wind speeds, differences between the open and gap in a) latent heat flux; b) sensible heat flux; c) Richardson number; and d) bulk exchange coefficient. Median differences (in regular font) and *p* values (in italic) from Wilcoxon rank-sum test are reported in each panel.

(Richardson number R_{iB}: Fig. 11c), bulk exchange coefficient (C_e: Fig. 11d), and air density and atmospheric pressure between open and gap as these fluxes also depend on these factors (Eqs. (6), and (7)). In addition to the median differences shown in Fig. 11, Table 3 provides absolute and relative effects of blowing snow on turbulent fluxes and variables involved in their calculation under the same wind regime, i.e., open winds in gap (see *AE* and *RE* metrics in Section 3.4). Relative effects in Table 3 quantitively show that blowing snow caused an average

Table 3
Absolute and relative effects of blowing snow on meteorological conditions and associated energy fluxes (see *AE* and *RE* metrics in Section 3.4 for equations). Calculations were done under the same wind regime in open and gap. Statistically significant variables are highlighted.

Energy flux/variable	Absolute effect	Relative effect (%)
T_a-T_s (°C)	–0.56 (°C)	–34
e_a-e_s (Pa)	2.70 (Pa)	–6
R_{iB}	–0.003 (-)	–40
C_e	0.0001 (-)	8
Air density (kg m^{-3})	0.0006 (kg m^{-3})	0.04
Atmospheric pressure (Pa)	0.00 (Pa)	0
Q_L (W m^{-2})	–0.30 (W m^{-2})	6
Q_S (W m^{-2})	–3.50 (W m^{-2})	–41

34% decrease in temperature gradient, 6% decrease in vapor pressure gradient, 40% decrease in air stability (R_{iB}), 8% increase in C_e, 6% increase in latent heat loss, and 41% decrease in sensible heat gain due to blowing snow fluxes. Changes in air density and atmospheric pressure due to blowing snow were negligible (Table 3), hence not presented in Fig. 11.

5. Discussion

5.1. Snowpack behavior between sites

The variation and evolution of the snow depth substantially differed between the sites over the study winter. The snowpack at the gap is characterized by comparatively higher snow depths and later snow disappearance date, which is in contrast to what Pomeroy and Granger (1997) observed in a clear-cut in Saskatchewan, Canada. However, the size of the gap plays an important role in snow accumulation and ablation in a gap, compared to the adjacent forest (Golding and Swanson, 1986; Pomeroy et al., 2002). Large gaps that are exposed to wind erosion reduce the overall snow accumulation compared to small gaps sheltered by trees, while small gaps (2–5 times the tree height diameter) are expected to accumulate a larger amount of snow (Troendle and Leaf, 1980; Swanson, 1988; Pomeroy and Gray, 1994; Pomeroy et al., 2002; Woods et al., 2006). Similarly, our gap site, with a size of approximately 2–3 times the typical tree height in the adjacent forest (13 m), accumulated more snow, due to sheltering from the wind (Fig. 3g). Conversely, the snowpack at the open site had lower snow depths and an earlier snow disappearance date. Although forest snow depths were consistently higher than that at the open site, the snow disappearance date was the same for both sites. The comparison of the snow depth variation with wind speed (Fig. 3a and g) suggests that the higher wind speeds played a significant role in shaping the snowpack at the open site. For instance, higher wind speeds promoted snow erosion (by enhancing blowing snow fluxes, Fig. 9), higher sublimation losses due to increased latent heat fluxes (Fig. 9 and 10), and densification of snow by wind compaction (Pomeroy and Gray, 1995; Pomeroy et al., 1998a; Vionnet et al., 2013; Jenicek et al., 2017; Mott et al., 2018). This resulted in lower snow depths at the open site. Although snow pit measurements were unfortunately not available in the study year due to logistical reasons, snow pits measurements carried out in early February 2020 reported a density of 440 kg m^{-3} in the open site and a density of 300 kg m^{-3} in the forest. These measurements suggest the mechanisms described above were present during the winter of 2020. In contrast, the dampened wind speeds in the forest and the gap (Fig. 3g) would have suppressed blowing snow transport and wind compaction. The comparatively lower snow depths in the forest compared to the gap could be due to the canopy interception losses in the forest. Our results show that large differences in energy transfers occurred whether the ground was fully or partially snow-covered at all the sites. The subsequent sections discuss in detail the difference in this energy partitioning between the sites during the three main periods of the winter: early winter, accumulation, and ablation.

5.1.1. Early winter period

The early winter period was characterized by a patchy snowpack less than 10 cm deep at all sites. The more variable mean snowpack temperatures in the open and comparatively steady variation in the gap, and even more in the forest, (Fig. 3c) is reflected by similar variations of energy fluxes at the sites (Fig. 5). Indeed, the more variable energy fluxes in the open resulted in more variable mean snowpack temperature, while steadier variations of energy fluxes in the forest resulted in more stable snowpack temperatures, with the gap site falling in between these two behaviors. Snowpack temperatures were more strongly correlated with air temperature under a thin snowpack, due to the reduced insulation, which is particularly prominent at the open site (Fig. 3b). Although forest and gap ground surface temperatures showed some freezing events early in the winter, the prolonged near-zero temperatures afterward indicate that even a thin layer of snow (< 10 cm) was sufficient to insulate the ground from freezing at these sites, despite the cold air temperatures (Fig. 3d). But in the open, more than 10 cm of snow layer was required to insulate the ground and stabilize its temperature. The energy partitioning shows a substantial ground heat influx received by the snowpack during early winter (Fig. 5 and 6), which is more pronounced in the open and the gap. For instance, the highest ground heat flux was reported during week 2 in the open. During this week, the sensible heat flux did not balance the radiative cooling (negative net longwave radiation); heat transfer from the soil to the snowpack and net shortwave radiation balanced the radiative cooling in the open, whereas, in the forest and gap, ground heat influxes were insufficient to fill the energy deficit. However, estimating energy fluxes during the early winter period is associated with higher uncertainties. One of the uncertainties comes from the possibility of shortwave penetration through a thin snowpack (Oke, 1987; Armstrong and Brun, 2008; Dewalle and Rango, 2008; Helgason and Pomeroy, 2012a). Significant solar energy can penetrate up to 10 cm depth in the snowpack, and can even warm the underlying surface (e.g., soil), which can bias the temperatures measured within and below a thin snowpack (Oke, 1987; Armstrong and Brun, 2008). High absorption of shortwave radiation in the surface layers of the snowpack can also increase the snow surface temperature (Dewalle and Rango, 2008). For a snowpack less than 10 cm like in early winter in our study, this could cause erroneous snowpack temperature measurements due to warming by direct solar radiation and associated inaccurate energy estimates. Moreover, Pomeroy and Granger (1997) and Armstrong and Brun (2008) reported that in the presence of a patchy snowpack, the snowpack could receive energy by advection through the overlaying air mass as a result of the radiant energy absorbed by the ground patches. This turbulent transfer of energy would neither be detected by the energy balance instrumentation nor in bulk approach calculations. This implies the challenges in the application of the energy balance equation for patchy, thin snowpacks.

Despite our effort to correct for a patchy snowpack by implementing the snow cover fraction approach and discarding energy estimates for very shallow daily snow depths (< 5 cm), the energy components calculated for the remaining days with thin snow depths (5–10 cm) might still suffer from these unaccounted processes.

5.1.2. Accumulation period

Throughout the accumulation period the snowpack was stable (> 10 cm), and so were the ground surface (snowpack base) temperatures (Fig. 3d). Snowpack base temperatures at gap and forest were consistently at 0 °C, indicating melting at the base, while temperatures at open were consistently lower than 0 °C. This suggests more frequent freezing at the base of the shallower snowpack and restricted infiltration in the open. A small ground heat influx received by the snowpack base throughout the accumulation period (Fig. 5a) indicates that the snowpack base was consistently colder than the soil beneath in the open. More variable energy flux exchanges resulted in more variable mean snowpack temperatures at the open (Fig. 5 and 3c). In contrast, energy exchanges were more attenuated within the forest, which resulted in more stable snowpack temperatures than in the open, with the gap snowpack falling in between. Radiative cooling due to longwave radiation losses was highest in the open. This, and the consistent negative net energy balance (positive grey bars in Fig. 5a) suggests a high cold content in the open, hence requiring more energy to warm the snowpack to 0 °C. Radiative cooling was lowest in the forest, and during weeks 6 and 9 the net longwave radiation even became an energy source for the forest snowpack (positive net longwave radiation in Fig. 5c), indicating more incoming longwave radiation within the forest, similar to the radiative paradox observed by Lundquist et al. (2013). This and the continuously positive net energy balance (negative grey bars in week 5–10 in Fig. 5c) in the forest suggest much lower cold content for the forest snowpack, hence requiring less energy to trigger melting. The gap snowpack shows an intermediate behavior between the open and forest. It received and lost more energy than the forest, but less than the open hence requiring more energy than the forest and less energy than the open to bring the snowpack to 0 °C. The high correlation between net longwave radiation and the net energy balance (Fig. 7b) suggests that radiative cooling was the most influential and crucial energy component during the accumulation period, i.e., determining how cold or warm the snowpack would be. Large temperature gradients between the atmosphere and snow surface and high wind speeds produced large sensible heat fluxes in the open that partly compensated for the radiative cooling during the accumulation period. The large negative latent heat fluxes suggest high sublimation rates at the open site. Not surprisingly, dampened wind speeds suppressed the turbulent fluxes at the forest and gap. Similar observations in radiation and turbulent fluxes were previously reported in open versus forested environments (e.g., Pomeroy and Granger, 1997; Reba et al., 2012; Roth and Nolin, 2017). Collectively, energy exchanges resulted in the coldest snowpack in the open, a comparatively warmer snowpack in the forest, and intermediate conditions at the gap, a conclusion also supported by the mean snowpack temperature variations (Fig. 5 and 3c).

5.1.3. Ablation period

From the beginning of the ablation period, the noticeable increase in net shortwave radiation and latent heat fluxes as the ablation period progressed at all sites suggests the increasing importance of these energy components for snowpack melting. The decrease in cold content and the warming and melting of the snowpack are reflected by the decline of longwave radiation losses and the positive net energy balance (negative grey bars in Fig. 5). In turn, the snowpack temperature gradually increased. The influence of net longwave radiation gradually diminished during the transition of the snowpack from the accumulation period to the ablation period and onward. However, during the last week of the ablation (week 14), net longwave radiation was positive in the forest, implying higher incoming longwave radiation within the forest, while it was slightly negative in the gap and markedly more negative in the open. Incoming longwave radiation is generally high within the forest due to longwave emittance by trees (Pomeroy and Granger, 1997; Lundquist et al., 2013). Inspection of individual fluxes shows that the increase of incoming longwave radiation, likely by the warming of trees is the reason for this positive net longwave radiation in week 14. Similar to the accumulation period, the sensible heat flux acted as an energy source during the ablation period. Latent heat fluxes were negative, implying a continuous sublimation (or evaporation) flux. Many studies documented the importance of net radiation for snowmelt in clear-cuts and forests (Pomeroy and Granger, 1997; Armstrong and Brun, 2008; Lundquist et al., 2013). Several studies also showed that the contribution of turbulent fluxes becomes particularly important late in the melt period (Mott et al., 2011a; Reba et al., 2012; Harder et al., 2017; Mott et al., 2017). Despite the high contribution of net shortwave radiation to the energy budget (Fig. 6f), our results show that the correlation between net shortwave radiation and net energy balance was secondary to that of latent heat fluxes at the open and gap (Fig. 7c). However, the opposite occurred in the forest, where shortwave radiation acted as the primary factor driving net energy balance, while the latent heat flux was secondary (Fig. 7c). Collectively, this thus implies that it is the difference in both shortwave radiation and latent heat flux that governs the difference in daily ablation between these sites. Another interesting finding in the ablation period is that despite the dissimilar snow depths and dissimilar energy budgets between open, forest, and gap sites, almost similar snow depth reduction rates were observed (Fig. 4).

5.2. Blowing snow

Hourly blowing snow fluxes measured at our site (0.002–8.6 g m^{-2} s^{-1}) are rather small compared to the measurements made elsewhere with the FlowCapt sensor, e.g. in the Swiss and French Alps (up to 90 g m^{-2} s^{-1}: Lehning and Fierz, 2008; Trouvilliez et al., 2015), Indian Himalayas (up to 40 g m^{-2} s^{-1}: Das et al., 2012), Central Asia (up to 192 g m^{-2} s^{-1}: Zhang et al., 2022), the Arctic region (up to 200 g m^{-1} s^{-1}: Jaedicke, 2001), and in Antarctica (up to 1200 g m^{-2} s^{-1}: Trouvilliez et al., 2014; Amory, 2020). Despite its relatively small magnitude, blowing snow events under snowfall-free conditions at our open site still account for substantial changes in snow depth over the course of accumulation period (deposition of 0.99 m and erosion of 0.83 m), with a net snow depth gain of 0.16 m equal to 29% of the peak winter snow depth recorded under the SR50 ultrasonics snow depth sensor. This recorded deposition may reflect the slightly elevated position of the terrain around the AWS, and possibly some influence of the AWS structure itself, in an otherwise predominantly exposed and erosional environment. This highlights the significance of blowing snow fluxes in altering snow-mass in the open fields of agro-forested landscapes with a cold-continental climate type.

5.2.1. Weather conditions associated with blowing snow

At our open site, the occurrence of blowing snow was found to be associated with cold dry air, elevated atmospheric pressure together with gusty weather, all typical of a passing cold front (Fig. 9). Our analysis shows a shift from negligible to a substantial increase in blowing snow fluxes above ~4 m s^{-1} wind speed (Fig. 8), which is in agreement with the threshold wind speed of 4–11 m s^{-1} found by Li and Pomeroy (1997) for dry snow transport in the Canadian prairies. They further noted that low temperatures produce snow covers with low cohesion and low transport threshold wind speeds which in turn increase the frequency of blowing snow events. However, our blowing snow measurements in the open showed no convincing correlations with air temperature or relative humidity. Our analysis shows that when sufficient snow is available on the ground, such as in the present case, the occurrence of blowing snow flux transport depends more on whether the snowpack is exposed to high wind speeds and low temperatures (Fig. 8d and e) rather than to snowfall. However, the occurrence of

blowing snow events can also be closely related to the state of the snowpack, such as surface layer density, snow grain shape and size, and surface hardness (Doorschot et al., 2004; Dewalle and Rango, 2008; Vionnet et al., 2014; Mott et al., 2018), which were not measured in this study.

5.2.2. Feedback effects of blowing snow

Our analysis shows that at an hourly scale, blowing snow fluxes have a substantial and rapid impact on changing the snow depths and modifying the energy budget in the open. Similar to previous studies (Déry et al., 1998; Bintanja, 2001a; Yang et al., 2010; Groot Zwaaftink et al., 2011; Barral et al., 2014; Vionnet et al., 2014; Le Toumelin et al., 2021) our analysis demonstrates thermodynamic feedback effects of blowing snow -wetting and cooling of the air above the snowpack due to blowing snow sublimation- which led to increased relative humidity, decreased vapor pressure gradient, and colder air temperature (Fig. 10). However, contrary to the aforementioned studies and the negative feedback observed on the vapor pressure gradient, the snowpack latent heat losses (surface sublimation) estimated by the bulk aerodynamic method still has a slight but insignificant increase during blowing snow events under no snowfall, even after correcting for the differences in wind speed between the two sites (Fig. 11). This happened because the cooling effect of blowing snow decreased the temperature gradient between the atmosphere and the snow surface (See Fig. 12), thereby decreasing air stability (R_{iB}). This led to an increase in the latent heat transfer coefficient (C_e: 8%) which surpassed the decrease in vapor pressure gradient (–6%) during blowing snow periods in the open (Table 3). Our analysis showed that the reduced temperature gradient during blowing snow periods also decreased the sensible heat gains to the snowpack during blowing snow events. Here the reduction in temperature gradient (–34%) surpassed the increase in C_e (8%), which led to reduced sensible flux gains. The reduced incoming longwave radiation reported during blowing snow periods can be ascribed to the cooling feedback of blowing snow sublimation, since the wetting feedback of blowing snow would rather increase the emissivity of the air and longwave radiation; and also because incoming longwave radiation is very sensitive to air temperature (Oke, 1987; Dewalle and Rango, 2008). Collectively, our analyses show that blowing snow is an important element in energy exchanges during the accumulation season in wind-exposed open areas of agro-forested landscapes with humid continental climates.

5.3. Limitations and way forward

One strong limitation of this study is the availability of a single measurement year. While the original design included two monitoring years, the data from the first winter suffered from large data gaps due to a power failure of the stations and the malfunction of some sensors. Future analyses would be useful to assess if the same patterns of energy partitioning persist over several years and to establish long-term trends between the open, forest, and gap snowpacks in agro-forested environments. Also, continuous SWE monitoring at the open and forest sites failed due to sensor malfunction. Concurrent snow depth and SWE measurements, also providing the snowpack density, would be useful to obtain a more complete understanding of the snowpack mass balance between the sites. For instance, even though a significant difference in snow depth was observed between the open and forest, both sites might have had the same SWE considering the wind-compacted denser snow at the open site. Therefore, deploying new passive SWE measuring sensors and snow pit measurements would be an added value in the future.

Another limitation in this study stems from the parameter uncertainty. For instance, a constant emissivity was used for all sites throughout the entire study period. Despite the possibility of varying emissivity over the course of snow season (Warren, 1982), obtaining reliable data for changing emissivity at sites proved challenging. Nevertheless, the anticipated impact on the results due to the use of constant emissivity, as opposed to varying values, is not expected to be significant (Armstrong and Brun, 2008). More than the emissivity, uncertainty in turbulent fluxes can have an impact on the results. In this context, the roughness length (z_0) has a significant influence on turbulent flux estimations by the bulk aerodynamic method. A future study that explores the sensitivity of this parameter across open, gap, and forest snowpacks would be necessary to obtain optimum z_0 values for the sites. Due to iterative nature and implementation complexity associated with the Monin-Obukhov scaling theory method (Stigter et al., 2018), we opted for the more straightforward and practical approach of employing the bulk aerodynamic method with Richardson number. However, it is also important to note that bulk aerodynamic method is associated with uncertainties related to the violation of logarithmic vertical wind profile and roughness length assumptions and very high stabilities over snow (Radić et al., 2017). A comparison of bulk aerodynamic method with different stability corrections based on Richardson number and Monin-Obhukhov scaling theory would provide more insights into the uncertainties involved in different methods.

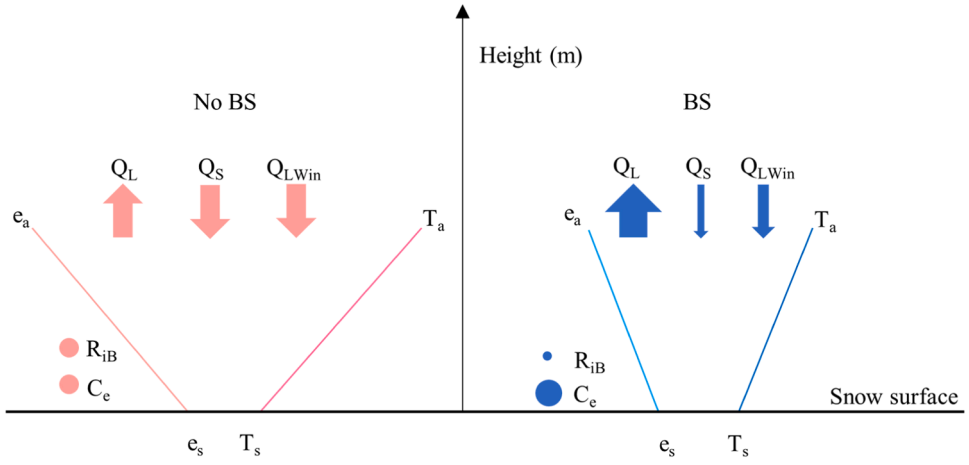

Fig. 12. Conceptual diagram of temperature gradient (T_a-T_s) and vapor pressure gradient (e_a-e_s) profiles and associated R_{iB}, C_e, and energy flux changes between no-blowing (No BS) and blowing snow (BS) events in the open. Size of the arrows and dots were adjusted to represent the increase or decrease of respective fluxes and variables during BS compared to No BS.

6. Conclusions

Our results show that there are considerable differences in energy fluxes between open, forest, and forest gap in an agro-forested landscape with a humid continental climate. Large variations in energy fluxes throughout the analyzed period caused more temporal variability in snowpack and ground temperatures in the open, whereas the comparatively small variations in energy fluxes caused more steady snowpack and ground temperatures in the forest and the gap exhibited an intermediate behavior. Net radiation dominated the snow surface energy balance between the sites, while turbulent fluxes were only significant at the wind-exposed open site. During the accumulation period, longwave radiation exerted a greater control on the variability of the daily net energy through radiative cooling. However, during the ablation period, latent heat fluxes and the absorption of solar radiation dominated the variability of the daily energy balance and snowpack melting.

Our analysis demonstrates that blowing snow fluxes have a substantial influence on changing snowpack dynamics in the open site at hourly scales. The frequency of blowing snow events occurring under snowfall-free conditions were three times higher than the events with concurrent snowfall which led to a net snow depth gain equivalent to 29% of the peak winter snow depth at the AWS location in open site. Our results suggest that when sufficient snow is available on the ground, the occurrence of blowing snow events depends more on the intensity of wind speed and cold air temperature rather than on concurrent snowfall. In addition to influencing the mass changes of the snowpack by accumulation and erosion processes, blowing snow modified the energy budget in the open through negative feedback effects. The observed increase in relative humidity and related decrease in vapor pressure gradient, and cooling of air temperature suggest a decrease in snowpack sublimation during blowing snow events. However, contrary to modelling (Déry et al., 1998; Bintanja, 2001a; Yang et al., 2010; Groot Zwaaftink et al., 2011; Vionnet et al., 2014; Le Toumelin et al., 2021) and observational (Bintanja, 2001b) studies that showed reduced snowpack sublimation during blowing snow events, our results rather showed that the decreased air stability in response to the decreased temperature gradient between the atmosphere and snowpack counterbalanced the reduced vapor pressure gradient and resulted in slightly increased latent heat (sublimation) losses from the snowpack during blowing snow. Furthermore, our analysis showed reduced influxes of sensible heat and longwave radiation to the snowpack in response to the blowing snow cooling feedback on the atmosphere. These results emphasize the significant role of blowing snow for the energy exchanges in large wind-exposed open areas in humid continental agro-forested landscapes.

Our study also highlights how dissimilar energy budgets can lead to comparable ablation patterns in open, forest, and forest gap environments. The ablation mainly differed between the sites due to the difference in latent heat fluxes and changes in shortwave radiation. The different snowpack and energy balance conditions between the open and forested patches of agro-forested landscapes highlighted in this study could have important implications for snowmelt infiltration patterns (Lundberg et al., 2016) and resulting catchment-scale hydrology (Aygün et al., 2020). For instance, our results show that the snowpack in the open was conductive to ground freezing and ice layer formation, while the forest snowpack and ground were warmer and devoid of ice layers. This has a great implication for infiltration patterns and thus the partition of meltwater between recharge and runoff in the region. As such, open agricultural areas are expected to produce more runoff, while forested areas would favor groundwater recharge, thereby influencing regional hydrology and flood regimes in the region. While these results are focused on southern Québec where such environments prevail, they have a broader implication for other cold agro-forested environments and they underscore the importance of incorporating blowing snow in physically based snow cover and hydrological models to correctly represent snow dynamics in such landscapes.

Funding

This study was financially supported by the Canada Research Chair program (grant number 231380) and the Natural Sciences and Engineering Research Council of Canada (NSERC discovery grant CRSNG-RGPIN-2015–03844) (Christophe Kinnard) and a doctoral scholarship from the Centre de Recherche sur les Interactions Bassins Versants-Écosytèmes Aquatiques (RIVE, Vasana Dharmadasa).

CRediT authorship contribution statement

Vasana Dharmadasa: Methodology, Formal analysis, Data curation, Writing – original draft. **Christophe Kinnard:** Conceptualization, Methodology, Formal analysis, Writing – review & editing, Supervision, Project administration, Funding acquisition. **Michel Baraër:** Writing – review & editing, Supervision.

Declaration of competing interest

The authors declare that they have no known competing financial interests or personal relationships that could have appeared to influence the work reported in this paper.

Data availability

Data will be made available on request.

Acknowledgments

The authors extend their appreciation to the members of GlacioLab for their help during fieldworks. Moreover, the authors are grateful to the Sainte-Marthe municipality, Québec, Canada.

Supplementary materials

Supplementary material associated with this article can be found, in the online version, at doi:10.1016/j.agrformet.2024.109915.

References

Amory, C., 2020. Drifting-snow statistics from multiple-year autonomous measurements in Adélie Land, East Antarctica. Cryosphere 14 (5), 1713–1725. https://doi.org/10.5194/tc-14-1713-2020.

Anderson, E.A. (1976). *A Point Energy and a Mass Balance Model of a Snow Cover*. Retrieved from NOAA Technical Report NWS 19, USA: https://repository.library.noaa.gov/view/noaa/6392.

Andreas, E.L., Horst, T.W., Grachev, A.A., Persson, P.O.G., Fairall, C.W., Guest, P.S., et al., 2010. Parametrizing turbulent exchange over summer sea ice and the marginal ice zone. Q. J. R. Meteorol. Soc. 136 (649), 927–943. https://doi.org/10.1002/qj.618.

Armstrong, R.L., Brun, E., 2008. Snow and Climate-Physical Processes, Surface Energy Exchange and Modeling. Cambridge University Press, New York, USA.

Aygün, O., Kinnard, C., Campeau, S., Krogh, S.A., 2020. Shifting hydrological processes in a Canadian agroforested catchment due to a warmer and wetter climate. Water (Basel) 12 (3), 739. https://doi.org/10.3390/w12030739.

Aygün, O., Kinnard, C., Campeau, S., Pomeroy, J.W., 2022. Landscape and climate conditions influence the hydrological sensitivity to climate change in eastern Canada. J. Hydrol. (Amst.) 615, 128595. https://doi.org/10.1016/j.jhydrol.2022.128595.

Bair, E.H., Davis, R.E., Dozier, J., 2018. Hourly mass and snow energy balance measurements from Mammoth Mountain, CA USA, 2011–2017. Earth. Syst. Sci. Data 10, 549–563. https://doi.org/10.5194/essd-10-549-2018.

Barral, H., Genthon, C., Trouvilliez, A., Brun, C., Amory, C, 2014. Blowing snow in coastal Adélie Land, Antarctica: three atmospheric-moisture issues. Cryosphere 8 (5), 1905–1919. https://doi.org/10.5194/tc-8-1905-2014.

Barry, R., Prévost, M., Stein, J., Plamondon, A.P., 1990. Application of a snow cover energy and mass balance model in a balsam fir forest. Water Resour. Res. 26 (5), 1079–1092.

Bintanja, R., 2001a. Modelling snowdrift sublimation and its effect on the moisture budget of the atmospheric boundary layer. Tellus A 53 (2), 215–232. https://doi.org/10.1034/j.1600-0870.2001.00173.x.

Bintanja, R., 2001b. Snowdrift sublimation in a katabatic wind region of the Antarctic ice sheet. J. Appl.d Meteorol. 40 (11), 1952–1966. https://doi.org/10.1175/1520-0450(2001)040<1952:SSIAKW>2.0.CO;2.
Boike, J., Roth, K., Ippisch, O., 2003. Seasonal snow cover on frozen ground: energy balance calculations of a permafrost site near Ny-Ålesund, Spitsbergen. J. Geophys. Res.: Atmos. 108 (D2), 8163. https://doi.org/10.1029/2001JD000939.
Brown, R.D., 2010. Analysis of snow cover variability and change in Québec, 1948–2005. Hydrol. Process. 24, 1929–1954. https://doi.org/10.1002/hyp.7565.
Broxton, P.D., Harpold, A.A., Biederman, J.A., Troch, P.A., Molotch, N.P., Brooks, P.D., 2015. Quantifying the effects of vegetation structure on snow accumulation and ablation in mixed-conifer forests. Ecohydrology. 8, 1073–1094. https://doi.org/10.1002/eco.1565.
Brun, E., Martin, E., Simon, V., Gendre, C., Coléou, C., 1989. An energy and mass model of snow cover suitable for operational avalanche forecasting. J. Glaciol. 35, 333–342. https://doi.org/10.1017/S0022143000009254.
Chritin, V., Bolognesi, R., Gubler, H., 1999. FlowCapt: a new acoustic sensor to measure snowdrift and wind velocity for avalanche forecasting. Cold Reg. Sci. Technol. 30 (1), 125–133. https://doi.org/10.1016/S0165-232X(99)00012-9.
Cierco, F.-X., Naaim-Bouvet, F., Bellot, H., 2007. Acoustic sensors for snowdrift measurements: how should they be used for research purposes? Cold Reg. Sci. Technol. 49 (1), 74–87. https://doi.org/10.1016/j.coldregions.2007.01.002.
Conway, J., Pomeroy, J., Helgason, W., Kinar, N., 2018. Challenges in modeling turbulent heat fluxes to snowpacks in forest clearings. J. Hydrometeorol. 19, 1599–1616. https://doi.org/10.1175/JHM-D-18-0050.1.
Conway, J.P., Cullen, N.J., 2013. Constraining turbulent heat flux parameterization over a temperate maritime glacier in New Zealand. Ann. Glaciol. 54 (63), 41–51. https://doi.org/10.3189/2013AoG63A604.
Das, R.K., Datt, P., Acharya, A., 2012. An assessment of the FlowCapt acoustic sensor for measuring snowdrift in the Indian Himalayas. J. Earth Syst. Sci. 121, 1483–1491.
Déry, S., Taylor, P., Xiao, J.B, 1998. The thermodynamic effects of sublimating, blowing snow in the atmospheric boundary layer. Boundary Layer Meteorol. 89 (2), 251–283. https://doi.org/10.1023/A:1001712111718.
Dewalle, D.R., Rango, A., 2008. Principles of Snow Hydrology. Cambridge University Press, New York, USA.
Doorschot, J.J., Lehning, M., Vrouwe, A., 2004. Field measurements of snow-drift threshold and mass fluxes, and related model simulations. Boundary Layer Meteorol. 113 (3), 347–368. https://doi.org/10.1007/s10546-004-8659-z.
Elder, K., Rosenthal, W., Davis, R.E., 1998. Estimating the spatial distribution of snow water equivalence in a montane watershed. Hydrol. Process. 12, 1793–1808.
Environment and Climate Change Canada. (2021). Hourly Data Report. Retrieved July 16, 2021 https://climate.weather.gc.ca/.
Essery, R., Pomeroy, J., 2004. Vegetation and topographic control of wind-blown snow distributions in distributed and aggregated simulations for an Arctic tundra basin. J. Hydrometeorol. 5, 735–744. https://doi.org/10.1175/1525-7541(2004)005<0735:VATCOW>2.0.CO;2.
Essery, R., Rutter, N., Pomeroy, J., Baxter, R., Stähli, M., Gustafsson, D., et al., 2009. SNOWMIP2 an evaluation of forest snow process simulations. Bull. Am. Meteorol. Soc. 90 (8), 1120–1135. https://doi.org/10.1175/2009BAMS2629.1.
Essery, R.L.H., Morin, S., Lejeune, Y., Ménard, C.B., 2013. A comparison of 1701 snow models using observations from an alpine site. Adv. Water Resour. 55, 131–148. https://doi.org/10.1016/j.advwatres.2012.07.013.
Golding, D.L., Swanson, R.H., 1986. Snow distribution patterns in clearings and adjacent forest. Water Resour. Res. 22 (13), 1931–1940.
Gootman, K.S., Hubbart, J.A., 2021. Rainfall, runoff and shallow groundwater response in a mixed-use, agro-forested watershed of the northeast, USA. Hydrol. Process. 35 (8), e14312. https://doi.org/10.1002/hyp.14312.
Groot Zwaaftink, C.D., Löwe, H., Mott, R., Bavay, M., Lehning, M., 2011. Drifting snow sublimation: a high-resolution 3-D model with temperature and moisture feedbacks. J. Geophys. Res.: Atmos. 116, D16107. https://doi.org/10.1029/2011JD015754.
Harder, P., Helgason, W.D., Pomeroy, J.W., 2018. Modeling the snowpack energy balance during melt under exposed crop stubble. J. Hydrometeorol. 19 (7), 1191–1214. https://doi.org/10.1175/JHM-D-18-0039.1.
Harder, P., Pomeroy, J.W., Helgason, W., 2017. Local-scale advection of sensible and latent heat during snowmelt. Geophys. Res. Lett. 44 (19), 9769–9777. https://doi.org/10.1002/2017GL074394.
Helgason, W., Pomeroy, J., 2012a. Problems closing the energy balance over a homogeneous snow cover during midwinter. J. Hydrometeorol. 13, 557–572. https://doi.org/10.1175/JHM-D-11-0135.1.
Helgason, W., Pomeroy, J.W., 2012b. Characteristics of the near-surface boundary layer within a mountain valley during winter. J. Appl. Meteorol. Climatol. 51 (3), 583–597. https://doi.org/10.1175/JAMC-D-11-058.1.
Hoelzle, M., Hauck, C., Mathys, T., Noetzli, J., Pellet, C., Scherler, M., 2022. Long-term energy balance measurements at three different mountain permafrost sites in the Swiss Alps. Earth Syst. Sci. Data 14 (4), 1531–1547. https://doi.org/10.5194/essd-14-1531-2022.
Hojatimalekshah, A., Uhlmann, Z., Glenn, N., Hiemstra, C., Tennant, C., Graham, J., et al., 2021. Tree canopy and snow depth relationships at fine scales with terrestrial laser scanning. Cryosphere 15, 2187–2209. https://doi.org/10.5194/tc-15-2187-2021.
Hopkinson, C., Pomeroy, J., Debeer, C., Ellis, C., and Anderson, A. (2012). *Relationships Between Snowpack Depth and Primary Lidar Point Cloud Derivatives in a Mountainous Environment*. Paper presented at the Remote Sensing and Hydrology, Jackson Hole, Wyoming, USA, 27–30 September 2010.
Hopkinson, C., Sitar, M., Chasmer, L., Treitz, P., 2004. Mapping snowpack depth beneath forest canopies using airborne lidar. Photogrammetric Eng. Remote Sens. 70 (3), 323–330.
Hydroinnova. (2019). SnowFox. Retrieved from http://hydroinnova.com/snow_water.html.
IAV Technologies. (2019). *User Guide-Operating Instructions for ISAW Sensors*. Retrieved from Tannay, Switzerland: https://www.isaw-products.com/.
Jacobs, J.M., Hunsaker, A.G., Sullivan, F.B., Palace, M., Burakowski, E.A., Herrick, C., et al., 2021. Snow depth mapping with unpiloted aerial system lidar observations: a case study in Durham, New Hampshire, United States. Cryosphere 15 (3), 1485–1500. https://doi.org/10.5194/tc-15-1485-2021.
Jaedicke, C., 2001. Acoustic snowdrift measurements: experiences from the FlowCapt instrument. Cold Reg. Sci. Technol. 32, 71–81.
Jenicek, M., Pevna, H., Matejka, O., 2017. Canopy structure and topography effects on snow distribution at a catchment scale: application of multivariate approaches. J. Hydrol. Hydromech. 66, 43–54. https://doi.org/10.1515/johh-2017-0027.
Jennings, K.S., Kittel, T.G.F., Molotch, N.P., 2018a. Observations and simulations of the seasonal evolution of snowpack cold content and its relation to snowmelt and the snowpack energy budget. Cryosphere 12 (5), 1595–1614. https://doi.org/10.5194/tc-12-1595-2018.
Jennings, K.S., Winchell, T.S., Livneh, B., Molotch, N.P., 2018b. Spatial variation of the rain–snow temperature threshold across the Northern Hemisphere. Nat. Commun. 9 (1), 1148. https://doi.org/10.1038/s41467-018-03629-7.
Jobin, B., Latendresse, C., Baril, A., Maisonneuve, C., Boutin, C., Côté, D, 2014. A half-century analysis of landscape dynamics in southern Québec, Canada. Environ. Monit. Assess. 186 (4), 2215–2229. https://doi.org/10.1007/s10661-013-3531-6.
Kinnard, C., Larouche, O., Demuth, M.N., Menounos, B., 2022. Modelling glacier mass balance and climate sensitivity in the context of sparse observations: application to Saskatchewan Glacier, western Canada. Cryosphere 16 (8), 3071–3099. https://doi.org/10.5194/tc-16-3071-2022.
Kuipers Munneke, P., van den Broeke, M.R., Reijmer, C.H., Helsen, M.M., Boot, W., Schneebeli, M., et al., 2009. The role of radiation penetration in the energy budget of the snowpack at Summit, Greenland. Cryosphere 3 (2), 155–165. https://doi.org/10.5194/tc-3-155-2009.
Lackner, G., Domine, F., Nadeau, D.F., Parent, A.C., Anctil, F., Lafaysse, M., et al., 2022. On the energy budget of a low-Arctic snowpack. Cryosphere 16 (1), 127–142. https://doi.org/10.5194/tc-16-127-2022.
Le Toumelin, L., Amory, C., Favier, V., Kittel, C., Hofer, S., Fettweis, X., et al., 2021. Sensitivity of the surface energy budget to drifting snow as simulated by MAR in coastal Adelie Land, Antarctica. Cryosphere 15 (8), 3595–3614. https://doi.org/10.5194/tc-15-3595-2021.
Lehning, M., Bartelt, P., Brown, B., Fierz, C., Satyawali, P., 2002. A physical SNOWPACK model for the Swiss avalanche warning Part II. Snow microstructure. Cold Reg. Sci. Technol. 35 (3), 147–167.
Lehning, M., Fierz, C., 2008. Assessment of snow transport in avalanche terrain. Cold Reg. Sci. Technol. 51 (2), 240–252. https://doi.org/10.1016/j.coldregions.2007.05.012.
Li, L., Pomeroy, J.W., 1997. Estimates of threshold wind speeds for snow transport using meteorological data. J. Appl. Meteorol. 36 (3), 205–213. https://doi.org/10.1175/1520-0450(1997)036<0205:EOTWSF>2.0.CO;2.
Liston, G.E., Haehnel, R.B., Sturm, M., Hiemstra, C.A., Berezovskaya, S., Tabler, R.D., 2007. Instruments and Methods-Simulating complex snow distributions in windy environments using SnowTran-3D. J. Glaciol. 53 (181), 214–256.
Liston, G.E., Sturm, M., 1998. A snow-transport model for complex terrain. J. Glaciol. 44 (148), 498–516. https://doi.org/10.3189/S0022143000002021.
Lundberg, A., Ala-Aho, P., Eklo, O., Klöve, B., Kværner, J., Stumpp, C., 2016. Snow and frost: implications for spatiotemporal infiltration patterns – a review. Hydrol. Process. 30 (8), 1230–1250. https://doi.org/10.1002/hyp.10703.
Lundquist, J.D., Dickerson-Lange, S.E., Lutz, J.A., Cristea, N.C., 2013. Lower forest density enhances snow retention in regions with warmer winters: a global framework developed from plot-scale observations and modeling. Water Resour. Res. 49, 6356–6370. https://doi.org/10.1002/wrcr.20504, 2013.
Luomaranta, A., Aalto, J., Jylhä, K., 2019. Snow cover trends in Finland over 1961–2014 based on gridded snow depth observations. Int. J. Climatol. 39 (7), 3147–3159. https://doi.org/10.1002/joc.6007.
Martin, E., Lejeune, Y., 1998. Turbulent fluxes above the snow surface. Ann. Glaciol. 26, 179–183. https://doi.org/10.3189/1998AoG26-1-179-183.
Mas, A., Baraer, M., Arsenault, R., Poulin, A., Préfontaine, J., 2018. Targeting high robustness in snowpack modeling for Nordic hydrological applications in limited data conditions. J. Hydrol. (Amst.) 564, 1008–1021.
Monin, A.S., and Yaglom, A.M. (1971). *Statistical Fluid Mechanics: Mechanics of Turbulence* (J. L. Lumley Ed. Vol. 1). USA: The Massachusetts Institute of Technology.
Mott, R., Egli, L., Grünewald, T., Dawes, N., Manes, C., Bavay, M., et al., 2011a. Micrometeorological processes driving snow ablation in an Alpine catchment. Cryosphere 5 (4), 1083–1098. https://doi.org/10.5194/tc-5-1083-2011.
Mott, R., Schirmer, M., Lehning, M., 2011b. Scaling properties of wind and snow depth distribution in an Alpine catchment. J. Geophys. Res. 116, D06106. https://doi.org/10.1029/2010JD014886.
Mott, R., Schlögl, S., Dirks, L., Lehning, M., 2017. Impact of extreme land surface heterogeneity on micrometeorology over spring snow cover. J. Hydrometeorol. 18 (10), 2705–2722. https://doi.org/10.1175/JHM-D-17-0074.1.
Mott, R., Vionnet, V., Grünewald, T., 2018. The seasonal snow cover dynamics: review on wind-driven coupling processes. Front. Earth. Sci. (Lausanne) 6, 197. https://doi.org/10.3389/feart.2018.00197.
Naaim-Bouvet, F., Bellot, H., Naaim, M., 2010. Back analysis of drifting-snow measurements over an instrumented mountainous site. Ann. Glaciol. 51 (54), 207–217. https://doi.org/10.3189/172756410791386661.
Oke, T.R., 1987. Boundary Layer Climates, 2nd edition ed. Routledge, New York, USA.

Paquotte, A., Baraer, M., 2021. Hydrological behavior of an ice-layered snowpack in a non-mountainous environment. Hydrol. Process 36 (1), e14433. https://doi.org/10.1002/hyp.14433.
Parajuli, A., Nadeau, D.F., Anctil, F., Alves, M., 2021. Multilayer observation and estimation of the snowpack cold content in a humid boreal coniferous forest of eastern Canada. Cryosphere 15 (12), 5371–5386. https://doi.org/10.5194/tc-15-5371-2021.
Pomeroy, J., Fang, X., Ellis, C, 2012. Sensitivity of snowmelt hydrology in Marmot Creek, Alberta, to forest cover disturbance. Hydrol. Process. 26 (12), 1891–1904. https://doi.org/10.1002/hyp.9248.
Pomeroy, J., and Gray, D.M. (1995). *Snowcover: accumulation, Relocation and Management*. Retrieved from Environment Canada, Saskatoon, Canada.
Pomeroy, J.W., Dion, K, 1996. Winter radiation extinction and reflection in a boreal pine canopy: measurements and modelling. Hydrol. Process. 10, 1591–1608.
Pomeroy, J.W., Granger, R.J., 1997. Sustainability of the western Canadian boreal forest under changing hydrological conditions-Snow accumulation and ablation. In: Paper presented at the Sustainability of Water Resources under Increasing Uncertainty (Proceedings of an international Symposium S1), Rabat, Morocco, 23 April–3 May 1997.
Pomeroy, J.W., Gray, D.M., 1994. In: *Sensitivity of snow relocation and sublimation to climate and surface vegetation.* Paper presented at the Snow and Ice Covers: Interactions with the Atmosphere and Ecosystems (Proceedings of Yokohama Symposia), Yokohama, Japan, July 1993.
Pomeroy, J.W., Gray, D.M., Brown, T., Hedstrom, N.R., Quinton, W.L., Granger, R.J., et al., 2007. The cold regions hydrological model: a platform for basing process representation and model structure on physical evidence. Hydrol. Process. 21 (19), 2650–2667. https://doi.org/10.1002/hyp.6787.
Pomeroy, J.W., Gray, D.M., Hedstrom, N.R., Janowicz, J.R., 2002. Prediction of seasonal snow accumulation in cold climate forests. Hydrol. Process. 16, 3543–3558. https://doi.org/10.1002/hyp.1228.
Pomeroy, J.W., Gray, D.M., Landine, P.G., 1993. The prairie blowing snow model: characteristics, validation, operation. J. Hydrol. (Amst.) 144, 165–192. https://doi.org/10.1016/0022-1694(93)90171-5.
Pomeroy, J.W., Gray, D.M., Shook, K.R., Toth, B., Essery, R.L.H., Pietroniro, A., et al., 1998a. An evaluation of snow accumulation and ablation processes for land surface modelling. Hydrol. Process. 12, 2339–2367.
Pomeroy, J.W., Parviainen, J., Hedstrom, N., Gray, D.M., 1998b. Coupled modelling of forest snow interception and sublimation. Hydrol. Process. 12, 2317–2337.
Prasad, R., Tarboton, D.G., Liston, G.E., Luce, C.H., Seyfried, M.S., 2001. Testing a blowing snow model against distributed snow measurements at Upper Sheep Creek, Idaho, United States of America. Water Resour. Res. 37 (5), 1341–1350.
Prévost, M., Barry, R., Stein, J., Plamondon, A.P., 1991. Snowmelt modeling in a balsam fir forest: comparison between an energy balance model and other simplified models. Canad. J. Forest Res. 21, 1–10. https://doi.org/10.1139/x91-001.
Price, A.G.S., Dunne, T., 1976. Energy balance computations of snowmelt in a subarctic area. Water Resour. Res. 12, 686–694.
Radić, V., Menounos, B., Shea, J., Fitzpatrick, N., Tessema, M.A., Déry, S.J., 2017. Evaluation of different methods to model near-surface turbulent fluxes for a mountain glacier in the Cariboo Mountains, BC, Canada. Cryosphere 11 (6), 2897–2918. https://doi.org/10.5194/tc-11-2897-2017.
Reba, M.L., Pomeroy, J., Marks, D., Link, T.E., 2012. Estimating surface sublimation losses from snowpacks in a mountain catchment using eddy covariance and turbulent transfer calculations. Hydrol. Process. 26 (24), 3699–3711. https://doi.org/10.1002/hyp.8372.
Roth, T.R., Nolin, A.W., 2017. Forest impacts on snow accumulation and ablation across an elevation gradient in a temperate montane environment. Hydrol. Earth. Syst. Sci. 21, 5427–5442. https://doi.org/10.5194/hess-21-5427-2017.
Rutter, N., Essery, R., Pomeroy, J., Altimir, N., Andreadis, K, 2009. Evaluation of forest snow processes models (SnowMIP2). J. Geophys. Res. 114. Paper 8.
Sena, N., Chokmani, K., Gloaguen, E., Bernier, M., 2017. Analyse multi-échelles de la variabilité spatiale de l'équivalent en eau de la neige (EEN) sur le territoire de l'Est du Canada. Hydrol. Sci. J. 62 (3), 359–377. https://doi.org/10.1080/02626667.2015.1022552.
Steiner, J.F., Litt, M., Stigter, E.E., Shea, J., Bierkens, M.F.P., Immerzeel, W.W., 2018. The importance of turbulent fluxes in the surface energy balance of a debris-covered glacier in the Himalayas. Front. Earth. Sci. (Lausanne) 6, 144. https://doi.org/10.3389/feart.2018.00144.
Stigter, E.E., Litt, M., Steiner, J.F., Bonekamp, P.N.J., Shea, J.M., Bierkens, M.F.P., et al., 2018. The importance of snow sublimation on a himalayan glacier. Front. Earth. Sci. (Lausanne) 6, 108. https://doi.org/10.3389/feart.2018.00108.
Swanson, R. (1988). *The effect of* in situ *evaporation on perceived snow distribution in partially clear-cut forests*. Paper presented at the Western Snow Conference 56: 87–92.
Tarboton, D.G., 1994. Measurements and Modeling of Snow Energy Balance and Sublimation from Snow. Retrieved from Utah State University, Logan, USA. https://digitalcommons.usu.edu/water_rep/61.
Troendle, C., Leaf, C., 1980. *Hydrology. An approach to water resources evaluation of non-point silviculture sources*. Environmental Research Laboratory, Athens, GA, USA.
Trouvilliez, A., Naaim-Bouvet, F., Bellot, H., Genthon, C., Gallée, H., 2015. Evaluation of the FlowCapt acoustic sensor for the aeolian transport of snow. J. Atmos. Ocean. Technol. 32, 1630–1641. https://doi.org/10.1175/JTECH-D-14-00104.1.
Trouvilliez, A., Naaim-Bouvet, F., Genthon, C., Piard, L., Favier, V., Bellot, H., et al., 2014. A novel experimental study of aeolian snow transport in Adelie Land (Antarctica). Cold Reg. Sci. Technol. 108, 125–138. https://doi.org/10.1016/j.coldregions.2014.09.005.
Valence, E., Baraer, M., Rosa, E., Barbecot, F., Monty, C, 2022. Drone-based ground-penetrating radar (GPR) application to snow hydrology. Cryosphere 16, 3843–3860. https://doi.org/10.5194/tc-16-3843-2022.
Varhola, A., Coops, N.C., Weiler, M., Moore, R.D., 2010. Forest canopy effects on snow accumulation and ablation: an integrative review of empirical results. J. Hydrol. (Amst.) 392, 219–233. https://doi.org/10.1016/j.jhydrol.2010.08.009.
Vionnet, V., Guyomarc'h, G., Lafaysse, M., Naaim-Bouvet, F., Giraud, G., Deliot, Y., 2018. Operational implementation and evaluation of a blowing snow scheme for avalanche hazard forecasting. Cold Reg. Sci. Technol. 147, 1–10. https://doi.org/10.1016/j.coldregions.2017.12.006.
Vionnet, V., Martin, E., Masson, V., Guyomarc'h, G., Naaim-Bouvet, F., Prokop, A., et al., 2014. Simulation of wind-induced snow transport and sublimation in alpine terrain using a fully coupled snowpack/atmosphere model. Cryosphere 8 (2), 395–415. https://doi.org/10.5194/tc-8-395-2014.
Vionnet, V., Naaim-Bouvet, F., Martin, E., Durand, Y., Bellot, H., Bel, C., et al., 2013. Occurrence of blowing snow events at an alpine site over a 10-year period: observations and modelling. Adv. Water Resour. 55, 53–63. https://doi.org/10.1016/j.advwatres.2012.05.004.
Warren, S.G., 1982. Optical properties of snow. Rev. Geophys. 20 (1), 67–89. https://doi.org/10.1029/RG020i001p00067.
Wilcoxon, F., 1945. Individual comparisons by ranking methods. Biometrics 1 (6), 80–83.
Winkler, R.D., Spittlehouse, D.L., Golding, D.L., 2005. Measured differences in snow accumulation and melt among clearcut, juvenile, and mature forests in southern British Columbia. Hydrol. Process. 19, 51–62. https://doi.org/10.1002/hyp.5757.
Woods, S.W., Ahl, R., Sappington, J., McCaughey, W., 2006. Snow Accumulation in Thinned Lodgepole Pine Stands, 235. Forest Ecology and Management, Montana, USA, pp. 202–211. https://doi.org/10.1016/j.foreco.2006.08.013.
Yang, J., Yau, M.K., Fang, X., Pomeroy, J.W., 2010. A triple-moment blowing snow-atmospheric model and its application in computing the seasonal wintertime snow mass budget. Hydrol. Earth Syst. Sci. 14 (6), 1063–1079. https://doi.org/10.5194/hess-14-1063-2010.
Zhang, W., He, J., Chen, A.a., Wu, X., Shen, Y., 2022. Observations of drifting snow using FlowCapt sensors in the Southern Altai mountains, Central Asia. Water (Basel) 14 (6), 845. https://doi.org/10.3390/w14060845.
Zheng, Z., Ma, Q., Qian, K., Bales, R.C., 2018. Canopy effects on snow accumulation: observations from lidar, canonical-view photos, and continuous ground measurements from sensor networks. Remote Sens. (Basel) 10, 1769. https://doi.org/10.3390/rs10111769.